J. Fluid Mech. (2001), *vol.* 429, *pp.* 343–380. Printed in the United Kingdom

© 2001 Cambridge University Press

Finite-amplitude internal wavepacket dispersion and breaking

By BRUCE R. SUTHERLAND

Department of Mathematical Sciences, University of Alberta, Edmonton, AB, Canada T6G 2G1

(Received 22 February 1999 and in revised form 6 September 2000)

The evolution and stability of two-dimensional, large-amplitude, non-hydrostatic internal wavepackets are examined analytically and by numerical simulations. The weakly nonlinear dispersion relation for horizontally periodic, vertically compact internal waves is derived and the results are applied to assess the stability of weakly nonlinear wavepackets to vertical modulations. In terms of Θ, the angle that lines of constant phase make with the vertical, the wavepackets are predicted to be unstable if $|\Theta| < \Theta_c$, where $\Theta_c = \cos^{-1}(2/3)^{1/2} \simeq 35.3^\circ$ is the angle corresponding to internal waves with the fastest vertical group velocity. Fully nonlinear numerical simulations of finite-amplitude wavepackets confirm this prediction: the amplitude of wavepackets with $|\Theta| > \Theta_c$ decreases over time; the amplitude of wavepackets with $|\Theta| < \Theta_c$ increases initially, but then decreases as the wavepacket subdivides into a wave train, following the well-known Fermi–Pasta–Ulam recurrence phenomenon.

If the initial wavepacket is of sufficiently large amplitude, it becomes unstable in the sense that eventually it convectively overturns. Two new analytic conditions for the stability of quasi-plane large-amplitude internal waves are proposed. These are qualitatively and quantitatively different from the parametric instability of plane periodic internal waves. The 'breaking condition' requires not only that the wave is statically unstable but that the convective instability growth rate is greater than the frequency of the waves. The critical amplitude for breaking to occur is found to be $A_{CV} = \cot\Theta(1 + \cos^2\Theta)/2\pi$, where A_{CV} is the ratio of the maximum vertical displacement of the wave to its horizontal wavelength. A second instability condition proposes that a statically stable wavepacket may evolve so that it becomes convectively unstable due to resonant interactions between the waves and the wave-induced mean flow. This hypothesis is based on the assumption that the resonant long wave–short wave interaction, which Grimshaw (1977) has shown amplifies the waves linearly in time, continues to amplify the waves in the fully nonlinear regime. Using linear theory estimates, the critical amplitude for instability is $A_{SA} = \sin 2\Theta/(8\pi^2)^{1/2}$. The results of numerical simulations of horizontally periodic, vertically compact wavepackets show excellent agreement with this latter stability condition. However, for wavepackets with horizontal extent comparable with the horizontal wavelength, the wavepacket is found to be stable at larger amplitudes than predicted if $\Theta \lesssim 45^\circ$. It is proposed that these results may explain why internal waves generated by turbulence in laboratory experiments are often observed to be excited within a narrow frequency band corresponding to Θ less than approximately 45°.

1. Introduction

It is well known that the cumulative effect of drag due to breaking internal waves has a significant impact on the strength and variability of the large-scale atmosphere and ocean circulations. To improve existing general circulation models it is necessary to improve our understanding of the processes that lead to internal wave breaking, and to make better predictions of where such breaking occurs. Linear theory predicts that waves may break when they approach an altitude where the speed of the mean flow equals the horizontal phase speed of the waves (Bretherton 1966; Booker & Bretherton 1967). Near this 'critical level' the phase lines of the waves tilt closer to the horizontal until, in the absence of diffusive effects, the waves become unstable due to convective overturning or shear instability. As pointed out recently by Broad (1995, 1999) and Shutts (1995, 1998), if the mean wind changes direction with height, the waves need not be trapped below a critical level and, indeed, may not break at all.

Even if the mean wind is uni-directional with height, finite-amplitude effects can act to adjust the height at which waves approaching a critical level ultimately break. This was first demonstrated by Jones & Houghton (1971) who used a numerical model to show that the mean flow, which is accelerated by the waves as they dissipate, acts to Doppler shift the frequency of the waves thus allowing wave penetration to greater heights. This phenomenon was examined in detail using a quasi-linear theory to model interactions between waves and the adjusted mean flow (Grimshaw 1975*a*; Fritts 1978, 1982; Dunkerton 1981).

In the absence of background shear there can be no critical levels. Nonetheless, atmospheric internal waves may break when they become saturated: as a consequence of the Eliassen–Palm theorem, which states that the vertical flux of momentum due to monochromatic, undamped internal waves does not change with height (Eliassen & Palm 1961), upward propagating internal waves increase in amplitude as the background density decreases, and the waves eventually grow to such a size that they break. Breeding (1972) and Jones & Houghton (1972) were the first to use nonlinear numerical models to simulate the effect of saturation and wave breaking in the absence of shear. They showed that, although linear theory correctly predicts the height at which wave breaking first occurs, the resulting acceleration of the mean flow rapidly leads to the spontaneous generation of a critical level which thereafter modifies the breaking process. Numerical investigations have since been performed to determine how the mean flow is affected by the breaking of internal waves in a background shear flow when the waves are both saturated and incident upon a critical level (Dunkerton 1982; Walterscheid 1984). In particular, in their study of large-amplitude, transient wavepackets, Fritts & Dunkerton (1984) showed that the frequency of the waves can shift due to interactions between waves and the wave-induced mean flow, and that this acts to 'dislocate' the critical level above its initial position. They referred to the frequency shift of the waves, which results from weakly nonlinear wave–wave interactions, as wave 'self-acceleration'.

Self-acceleration can significantly affect the evolution of internal waves whether or not a critical level is present. In particular, it has been shown that self-acceleration can act to enhance the transmission of large-amplitude transient wavepackets across a reflecting level (Sutherland 1999, 2000).

The purpose of this paper is to examine the evolution and stability of large-amplitude internal waves in the absence of saturation and critical levels. To this end, the propagation of waves is studied in uniformly stratified Boussinesq fluid with no shear. It is shown that if a quasi-plane internal wavepacket is of sufficiently large

amplitude, but not so large that the waves are initially overturning, the wavepacket may nonetheless break as it evolves due to the effects of self-acceleration.

Instability due to self-acceleration is different from parametric instability. It is now well established that a plane periodic internal wave is unstable due to parametric instabilities in which secondary waves of half the primary wave frequency grow in amplitude through resonant interactions with the primary wave (Hasselmann 1967; Mied 1976; Drazin 1977; Klostermeyer 1991; Lombard & Riley 1996). (For a review of wave interaction theory in general, see Phillips 1981.) Instability of this kind has been observed in laboratory experiments (Benielli & Sommeria 1996) and in numerical simulations (Bouruet-Aubertot, Sommeria & Staquet 1995).

In particular, monochromatic internal waves are unstable even at infinitesimally small amplitudes provided the timescale of the instability is smaller than the diffusive timescale. Of course, one should not conclude from this that internal waves cannot exist; wavebreaking occurs only after the unstable waves grow to sufficiently large amplitude, a process that may last much longer than the propagation and diffusion timescales.

In any realistic geophysical circumstance internal waves are not perfectly monochromatic, and therefore the waves disperse as they propagate. Finite-amplitude wavepackets must be susceptible to the effects of nonlinear dispersion. The numerical simulations presented here demonstrate that weakly nonlinear wave–mean flow interactions dominate the dynamics governing the evolution of large-amplitude quasi-plane internal waves.

In weakly nonlinear theory, a quasi-plane wavepacket may be unstable due to modulations of the large-amplitude waves. Whether or not instability occurs may be assessed from the weakly nonlinear dispersion relation of the wave by using Whitham's equations (see Whitham 1974, § 15.1, and Debnath 1994, § 7.6). Whitham's result, as relevant to the discussion here, may be summarized as follows: if the weakly nonlinear, one-dimensional dispersion relation of waves with amplitude A is given by

$$\omega = \omega_0(k) + \omega_2(k)A^2, \tag{1.1}$$

where k is the wavenumber, ω is the frequency and $\omega_0(k)$ is the linear dispersion relation, then the wavepacket is unstable if $\omega_2\omega_0'' < 0$ (Whitham 1974). From this it follows, for example, that deep water waves are unstable at all wavenumbers, as indeed is well established by experiment and theory (Benjamin 1967; Benjamin & Feir 1967; Whitham 1967; Lake *et al.* 1977).

In weakly nonlinear theory, if a wavepacket of fundamental wavenumber k_0 is unstable to finite-amplitude modulations, it will grow in amplitude to a maximum limit. The energy is then transferred to waves of wavenumber near k_0 which later transfer this energy back to the fundamental wavenumber. These dynamics are a manifestation of the 'Fermi–Pasta–Ulam' recurrence phenomena (Fermi, Pasta & Ulam 1974). Modulational instability does not necessarily lead to wave breaking.

Wave instability due to self-acceleration differs qualitatively from parametric and modulational instability in that it results from a resonant interaction between waves and the wave-induced mean flow. The resonance occurs when the waves are of such large amplitude that the wave-induced mean flow is at least as large as the horizontal group velocity of the waves. Such instability is quantitatively different from parametric and modulational instability in that the waves are predicted to be unstable only if their amplitude, in general, exceeds a finite threshold. In contrast, there are no lower bounds on the amplitude necessary for parametric and modulational instability to occur.

In § 2 the linear and weakly nonlinear theory of internal waves is reviewed and the weakly nonlinear dispersion relation for horizontally periodic, vertically compact internal waves is explicitly derived. The modulational stability criterion for such waves is thus determined. Specifically it is shown that a wavepacket is unstable if the absolute value of the ratio of its vertical to horizontal wavenumber is less than $1/\sqrt{2} \simeq 0.71$. (Waves with the ratio equal to $1/\sqrt{2}$ correspond to wavepackets propagating with the fastest vertical group velocity.) For such non-hydrostatic waves, the lines of constant phase tilt at an angle $\Theta \lesssim 35^\circ$ to the vertical. The theory deriving the critical amplitude for overturning waves is reviewed and a new condition is proposed that predicts at what amplitude convective breaking will occur. By identifying the wave-induced mean flow with the pseudomomentum of internal waves, for which an explicit analytic formula is known, the critical amplitude at which waves are unstable due to self-acceleration is determined.

These predictions are compared with the results of fully nonlinear numerical simulations. The numerical model is described in detail in § 3. In § 4, the results of representative simulations are presented to show how the structure of internal waves changes as a function of their amplitude, initial tilt of their phase lines to the vertical and their spatial extent. Simulations are performed of doubly periodic, horizontally periodic/vertically compact, and horizontally and vertically compact wavepackets. Parametric instability is observed for doubly periodic waves. However, spectral energy transfer diagnostics demonstrate that interactions between the fundamental waves and the wave-induced mean flow dominate over interactions between the fundamental and its harmonics when the wavepacket is vertically compact. In agreement with the modulational stability criterion derived in § 2, wavepackets are found to be unstable if the magnitude of their vertical wavenumbers is sufficiently small, and the wavepackets are stable to finite-amplitude modulations otherwise. In § 5 the results of a range of simulations are presented in which the stability of the wavepackets to overturning and breaking is evaluated. For simulations of horizontally periodic, vertically compact wavepackets, the stability regimes agree well with the self-acceleration condition derived in § 2. Horizontally and vertically compact wavepackets are generally found to be stable at larger amplitudes than predicted by the self-acceleration condition if the magnitude of their vertical wavenumber is moderately less than their horizontal wavenumber. The application of these results to experiments on wave generation in stratified turbulence is discussed in § 6.

2. Internal wave theory and stability criteria

Internal waves are examined in uniformly stratified Boussinesq fluid with no shear. In the Boussinesq approximation, density variations are assumed to be negligible except for their effects upon buoyancy. The approximation is applicable to internal waves in the ocean and may be applied to atmospheric waves over vertical lengthscales smaller than the density scale height of the atmosphere, on the order of 10 km (Spiegel & Veronis 1960). Internal waves that propagate upward over larger vertical distances (i.e. waves that are non-Boussinesq) grow significantly in amplitude. A complete study of wave breaking in the atmosphere must include such anelastic effects. Likewise, the interaction of internal waves with critical levels is an important factor governing whether and where wave breaking occurs. In this paper these processes are neglected in order to demonstrate clearly that the wave breaking occurs in the absence of saturation and critical levels.

2.1. *Basic equations*

It is convenient to represent the degree of stratification in terms of the squared buoyancy frequency N_0^2, which in the Boussinesq approximation is proportional to the vertical gradient of the background density. Explicitly,

$$N_0^2 = -(g/\rho_0)\,\mathrm{d}\bar{\rho}/\mathrm{d}z, \tag{2.1}$$

in which $\bar{\rho}(z)$ is the background profile of density, ρ_0 is a reference value of density and g is the gravitational acceleration. The background density decreases linearly with height if N_0 is constant. For atmospheric motion, N_0^2 is proportional to the vertical gradient of the background potential temperature but, for convenience, the definition given by (2.1) will be used throughout.

In uniformly stratified inviscid fluid which is two-dimensional, the fully nonlinear equations of motion for the fields of vorticity ζ and vertical displacement ξ are

$$\frac{\mathrm{D}\zeta}{\mathrm{D}t} = N_0^2\frac{\partial\xi}{\partial x} + \mathscr{D}_\zeta \tag{2.2}$$

and

$$\frac{\mathrm{D}\xi}{\mathrm{D}t} = w + \mathscr{D}_\xi. \tag{2.3}$$

With N_0 constant, ξ is related to the fluctuation density field, ρ, by the relation

$$\rho = -\bar{\rho}'(z)\xi = \left(\frac{\rho_0}{g}N_0^2\right)\xi. \tag{2.4}$$

$\mathrm{D}/\mathrm{D}t = \partial/\partial t + u\partial/\partial x + w\partial/\partial z$ is the material derivative, and u and w are the horizontal and vertical components, respectively, of the velocity field. The diffusion operators $\mathscr{D}_\zeta$ and $\mathscr{D}_\xi$ are neglected in the theory below, but are necessarily employed in the numerical model, as discussed in the next section.

This study is concerned primarily with the dynamics of non-hydrostatic waves, that is, waves with intrinsic frequencies close to the buoyancy frequency. Because the Coriolis frequency f is typically two orders of magnitude smaller than the buoyancy frequency of the atmosphere, Coriolis forces are neglected.

A Boussinesq fluid is incompressible and therefore the velocity fields may be expressed in terms of the streamfunction ψ:

$$u = -\frac{\partial\psi}{\partial z} \tag{2.5}$$

and

$$w = \frac{\partial\psi}{\partial x}. \tag{2.6}$$

Thus, in terms of ψ, the basic state fields are given by

$$\zeta = -\nabla^2\psi. \tag{2.7}$$

and

$$\frac{\mathrm{D}\xi}{\mathrm{D}t} = \frac{\partial\psi}{\partial x}. \tag{2.8}$$

The initial conditions for (2.2) and (2.3) are given in terms of the streamfunction:

$$\psi(x,z) = \Psi(x,z)\exp\left[\mathrm{i}(k_x x + k_z z)\right] + \text{c.c.}, \tag{2.9}$$

in which $\Psi(x,z)$ prescribes the form of the wavepacket envelope and c.c. denotes

the complex conjugate. The horizontal wavenumber k_x is set to be positive and the vertical wavenumber k_z is set to be negative, so that in time the wavepacket propagates upward and to the right.

The wavepackets considered here are either doubly periodic (monochromatic, plane waves) with

$$\Psi = A_0, \tag{2.10}$$

horizontally periodic and vertically compact with

$$\Psi \equiv \Psi_{\rm PW}(z) = A_0 \exp(-|z|/\sigma_z), \tag{2.11}$$

or horizontally and vertically compact with

$$\Psi \equiv \Psi(x,z) = A_0 \exp(-|z|/\sigma_z) \exp(-x^2/2\sigma_x^2). \tag{2.12}$$

Note, the meaning of 'compact' is not used here in the strict mathematical sense, but is meant to indicate that the amplitude of the waves is vanishingly small except within a region of finite extent. For propagating waves, the initial vertical displacement field is defined in terms of the streamfunction by $\xi = -(k_x/\Omega)\psi$, in which Ω is the wave frequency.

In each case, $A_\psi \equiv 2A_0$ is the streamfunction amplitude and σ_x and σ_z are the horizontal and vertical extents of the wavepacket, respectively. Note that (2.10) is equivalent to setting σ_x and σ_z to be infinitely large, and (2.12) is equal to (2.11) in the limit as σ_x becomes infinitely large. Typically the envelope is set to be sufficiently large that it is a quasi-plane wavepacket. That is, $\sigma_x \gg 1/|k_x|$ and $\sigma_z \gg 1/|k_z|$.

Vertically compact wavepackets are set to decay exponentially with height for historical reasons: as an internal wavepacket develops from a transient forcing mechanism, such as variable flow over topography, convection, or shear instability, the leading and trailing edges are predicted to decay exponentially with distance from the centre of the wavepacket (see, for example, McIntyre & Weissman 1978; Sutherland, Caulfield & Peltier 1994). The horizontal envelope of a horizontally compact wavepacket is set to be the typical shape of a Gaussian. The qualitative results of these simulations are not expected to depend sensitively upon the detailed structure of the wavepacket envelopes.

The boundary conditions on (2.2) and (2.3) are set to be periodic in the directions where the waves are periodic and the domain is infinite in extent in the direction where the waves are compact.

The choice of length and timescales is arbitrary. Typically quantities are given here in non-dimensional form based on the horizontal wavelength, $\lambda_x = 2\pi/k_x$, representing the characteristic lengthscale and the buoyancy period, $T = 2\pi/N_0$, representing the characteristic timescale.

The initial state for doubly periodic, horizontally periodic/vertically compact, and horizontally and vertically compact wavepackets is shown in figures 1(*a*), 1(*b*) and 1(*c*), respectively. In (*b*) and (*c*), the vertical extent of the wavepacket is given by $\sigma_z = 10/k_x$ and in (*c*) the horizontal extent of the horizontally compact wavepacket is given by $\sigma_x = 10/k_x$. The streamfunction amplitude of each wavepacket is given by $A_\psi = 0.1N_0/k_x^2$ which corresponds to a maximum vertical displacement of $A_\xi = 0.017\lambda_x$. The contours illustrated by the grey-scale in each figure show the normalized vertical displacement field $\xi(x,z)/\lambda_x$. Other aspects of this figure are described later.

2.2. *Linear dispersion relation*

For small-amplitude waves, the advection terms in the material derivatives in (2.2) and (2.3) are neglected. For plane periodic waves, substitution of (2.10) into the

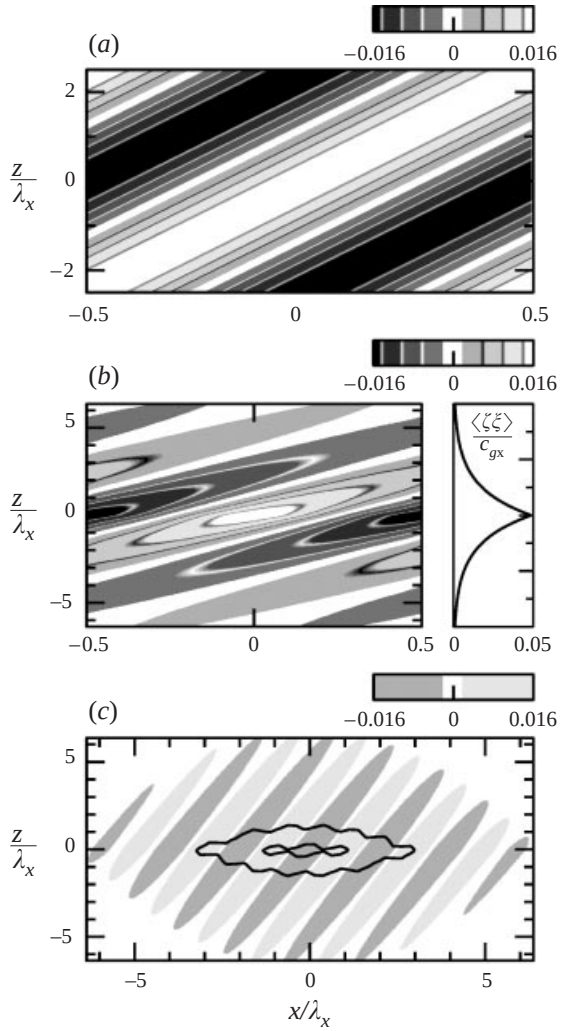

FIGURE 1. Typical initial state of (*a*) doubly periodic, (*b*) horizontally periodic/vertically compact, and (*c*) horizontally and vertically compact wavepackets. In each case the amplitude $A = A_\xi/\lambda_x = 0.017$ and $k_z = -0.4k_x$. In (*a*), (*c*) and the left-hand panel of (*b*) the grey scale shows the normalized vertical displacement field $\xi(x,z)/\lambda_x$. The x- and z-axes in these plots are scaled by λ_x. The right-hand panel in (*b*) shows the pseudomomentum profile normalized by the predicted horizontal group velocity. In (*c*), contours of the normalized and locally averaged pseudomomentum field are shown superimposed on the contours of ξ/λ_x. Contours are shown by intervals of 0.02. In (*a*), the pseudomomentum profile (not shown) is constant.

resulting equation and neglecting diffusion yields an eigenvalue problem from which the dispersion relation is found:

$$\Omega = N_0 k_x/|\boldsymbol{k}| = N_0 \cos\Theta, \tag{2.13}$$

in which Ω is the (intrinsic) frequency of the waves, $|\boldsymbol{k}|^2 = k_x^2 + k_z^2$ and $\Theta = \cos^{-1}(\Omega/N_0) = \tan^{-1}(|k_z/k_x|)$ is the angle at which lines of constant phase tilt from the vertical (for example, see Gill 1982, §6.5). The corresponding eigenfunctions yield the 'polarization relations' from which, for example, the amplitude of the vertical displacement field, A_ξ, may be determined in terms of the streamfunction

amplitude A_ψ:

$$A_\xi \simeq A_\psi / c_{px}, \tag{2.14}$$

in which the horizontal phase speed $c_{px} \equiv \Omega/k_x = N_0 \cos\Theta/k_x$. It is convenient to define the non-dimensional amplitude A as the ratio of the maximum vertical displacement to the horizontal wavelength. Explicitly

$$A = \frac{A_\xi}{\lambda_x} = \frac{1}{2\pi}\frac{A_\psi k_x}{N_0}|\boldsymbol{k}|. \tag{2.15}$$

These relationships also hold for quasi-plane wavepackets such as those given by (2.11) and (2.12) with $|k_x\sigma_x| \gg 1$ and $|k_z\sigma_z| \gg 1$. The velocity at which such wavepackets translate as a whole is given by the group velocity (for example, see Gill 1982, § 6.6):

$$(c_{gx}, c_{gz}) = N_0 \frac{k_z}{|\boldsymbol{k}|^3}(k_z, -k_x).$$

In particular, in terms of N_0 and k_x the magnitude of each component of the group velocity is given by

$$(|c_{gx}|, |c_{gz}|) = \frac{N_0}{k_x}\cos\Theta \sin\Theta(\sin\Theta, \cos\Theta). \tag{2.16}$$

A quantity examined in detail here is the wave-induced mean flow. For small-amplitude, horizontally periodic waves, the wave-induced mean flow is negligibly different from the second-order-accurate expression for the wave pseudomomentum

$$M(z) = -\langle \zeta \xi \rangle, \tag{2.17}$$

in which the angle brackets denote the horizontal average over the domain (Shepherd 1990; Scinocca & Shepherd 1992). Thus the wave-induced mean flow may be diagnosed from the basic-state vorticity and vertical displacement fields. Even for moderately large-amplitude waves, Sutherland (1996) has shown that this estimate is a good approximation to the actual wave-induced mean flow. In part, this is because the non-dimensional amplitude A of stable waves is typically less than 0.1, and therefore higher-order corrections to (2.17) are negligibly small.

From the polarization relations, the magnitude of the wave-induced mean flow, A_M, may be estimated from the characteristics of the initial wavepacket. Explicitly,

$$A_M = \tfrac{1}{2}A_\psi^2 \frac{|\boldsymbol{k}|^3}{N_0}.$$

Using (2.13) and (2.15) gives

$$A_M = 2\pi^2 A^2 \frac{N_0}{k_x}\sec\Theta. \tag{2.18}$$

For horizontally compact waves, it is convenient to define the field

$$M(x,z) = -\langle \zeta \xi \rangle_{\lambda_x}, \tag{2.19}$$

which is determined at each point (x,z) by horizontally averaging the product $\zeta\xi$ over one horizontal wavelength centred about x. Note that for horizontally periodic waves, $M(x,z)$ is independent of x.

The right-hand panel of figure 1(b) shows the profile of the normalized wave-induced mean flow $M(z)$ corresponding to the wave shown in the left-hand panel with $k_z = -0.4k_x$. The predicted horizontal group velocity c_{gx} is used as a normalization

factor. Superimposed on the vertical displacement field in figure 1(*c*) are contours of the normalized $M(x,z)$ field shown by intervals of 0.02.

2.3. *Weakly nonlinear dispersion and modulational stability*

The dispersion relation of moderately large-amplitude wavepackets must be modified to account for the effects of weakly nonlinear dispersion. Take, for example, the case of a one-dimensional wavepacket, in which the linear dispersion relation is $\omega_0 = \omega_0(k)$. (Here the orientation of the wavenumber k is arbitrary.) Typically the weakly nonlinear dispersion relation may be written in the form

$$\omega = \omega_0 + A^2\omega_2 + O(A^4) \tag{2.20}$$

where $\omega_2 = \omega_2(k)$ is the second-order finite-amplitude correction to the dispersion relation. Following Whitham's stability theory (Whitham 1965, 1974), the wavepacket is found to be stable or unstable depending on whether the quantity $\omega_2\omega_0''$ is positive or negative, respectively. (The primes denote derivatives with respect to k.) In the former case, modulation of the wavepacket obeys a hyperbolic system of equations; the initial wavepacket splits into two separate disturbances propagating with group velocities c_{g+} and c_{g-} given by

$$c_{g\pm} = \omega_0'(k) \pm A\left[\omega_2\omega_0''\right]^{1/2} + O(A^2). \tag{2.21}$$

In the latter case, the modulation of the wavepacket obeys an elliptic system of equations, hence the wavepacket envelope grows in time.

In Appendix A the weakly nonlinear dispersion relation for horizontally periodic, vertically compact (and unbounded) internal waves is derived. In this derivation $\omega_0 \equiv \Omega$ in (2.13) with $k \equiv k_z$ and k_x fixed. From (A 19), it is found that

$$\omega_2 = \omega_0 2\pi^2/\cos^2\Theta, \tag{2.22}$$

which is always positive. Thus modulational instability is predicted to occur if the vertical group velocity decreases with increasing vertical wavenumber. In terms of Θ, the wavepacket is therefore unstable if

$$|\Theta| < \tan^{-1}(1/\sqrt{2}) \simeq 35^\circ. \tag{2.23}$$

The numerical simulations presented in § 4 are in excellent agreement with this prediction.

The modulational stability of a vertically confined large-amplitude internal wavepacket that is horizontally modulated has been considered by Grimshaw (1975*b*, 1977). He found that the second-order correction to the weakly nonlinear dispersion relation is given by

$$\omega_2 = -12\frac{k_x}{c_{px}}\frac{\sigma^6}{1-4\sigma^6}, \tag{2.24}$$

where $\sigma = c_{gx}/c_{px}$ is the ratio of the horizontal group to phase speed. Thus such wavepackets are unstable to horizontal modulations if

$$\omega_2\frac{\partial^2\omega_0}{\partial k_x{}^2} = 36\frac{\cos^2\Theta\sin^8\Theta}{1-4\sin^6\Theta} < 0.$$

In terms of Θ, instability occurs if

$$|\Theta| > \sin^{-1}(2^{-1/3}) \simeq 53^\circ. \tag{2.25}$$

The modulational instability of the wavepacket does not guarantee wave breaking.

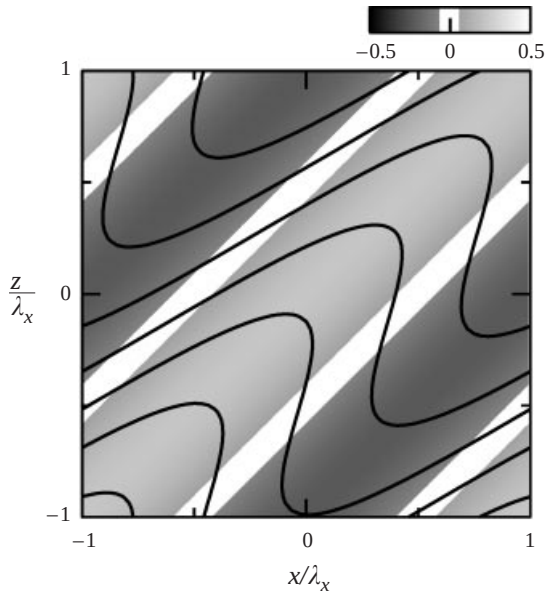

FIGURE 2. Normalized vertical displacement field of an overturning doubly periodic wave. Isopycnal surfaces are superimposed. The wave is shown with $k_z = -k_x$ and amplitude $A \simeq 0.23$.

On the contrary, a large body of theoretical and numerical work has demonstrated that moderately large-amplitude wavepackets initially grow in amplitude but then decrease in amplitude as waves grow in the sideband frequencies. Subsequently, energy is taken up back into the fundmental waves and the process repeats, following the modulation–demodulation cycle known as the Fermi–Pasta–Ulam recurrence phenomenon (Fermi *et al.* 1974; Zabusky & Kruskal 1965; Benjamin & Feir 1967).

2.4. *Wave-breaking criteria*

An internal wavepacket is statically unstable if dense fluid is lifted by the waves to such a degree that it overlies less dense fluid somewhere in the wavefield (e.g. Gill 1982, § 8.10). This is illustrated in figure 2, which shows isopycnal surfaces superimposed on the vertical displacement field of a doubly periodic internal wave. The wave is of such large amplitude in this example that the fluid is statically unstable along a diagonal band situated below the contour of maximum vertical displacement and above the contour of minimum vertical displacement.

An explicit formula for the critical amplitude at which a periodic wave train is unstable is found by requiring that the sum of the vertical gradients of the background density and fluctuation density field is positive: $\partial(\bar{\rho}(z) + \rho(x,z))/\partial z > 0$. Defining

$$\Delta N^2 \equiv \Delta N^2(x,z) = -\frac{g}{\rho_0}\frac{\partial \rho}{\partial z}, \tag{2.26}$$

the condition that the wavefield is statically unstable is

$$\Delta N^2(x,z) < -N_0^2 \tag{2.27}$$

for some (x,z).

Using (2.4), (2.15), and (2.13), the amplitude of the ΔN^2 field is

$$A_{\Delta N^2} = 2\pi A N_0^2 \tan\Theta, \tag{2.28}$$

and the critical (non-dimensional) amplitude at which plane internal waves are statically unstable is therefore

$$A_{OT} = \frac{1}{2\pi}\cot\Theta. \tag{2.29}$$

Hereafter, a wavepacket with initial amplitude $A > A_{OT}$ is said to satisfy the 'overturning condition'. Note that A_{OT} becomes infinitely large as $\Theta \to 0$.

A plane wave that is statically unstable is susceptible to the development of convective instabilities. However, the overturning condition alone does not guarantee that the wavepacket will convectively mix. If the period of the wave motion is much shorter than the timescale for the growth of convective instability, then statically unstable regions are transient and convective instability does not have time to develop significantly before the periodic wave motion acts to restore stability to the region. For example, the unstable region in figure 2 will be stable after half a wave period provided convective mixing has not had time to develop. If, however, the timescale for convection is much shorter than the period of the wave evolution, convective wave breaking is expected. The overturning condition is a necessary but not sufficient condition for the latter process to occur.

The timescale of convective instability is estimated using Rayleigh–Taylor theory (Rayleigh 1883; Taylor 1950; Drazin & Reid 1981, §44.2). For a linearly stratified Boussinesq fluid bounded above and below over a depth H, the fastest growing normal mode disturbance of horizontal wavenumber α develops on an e-folding timescale $1/\sigma$ where

$$\sigma = (-N^2)^{1/2}\left[1 + \left(\frac{\pi}{H\alpha}\right)^2\right]^{-1}. \tag{2.30}$$

The growth rate is real-valued if the fluid is statically unstable, that is, if $N^2 < 0$. The fastest growing disturbances are the infinitesimally small ones (i.e. $\alpha \to \infty$, or equivalently $H \to \infty$) in which case $\sigma \simeq (-N^2)^{1/2}$. Note that the maximum growth rate is independent of the depth of the overturning region. The local value of the squared buoyancy frequency in an internal wave field is $N_0^2 + \Delta N^2$. We define $N^2 = N_0^2 + \Delta N^2$, and note from (2.27) that $N^2 < 0$ if the waves are overturning. Then, using (2.26) and (2.4), the maximum growth rate is given in terms of the amplitude of the vertical displacement field by

$$\sigma_{\max} = N_0(|k_z|A_\xi - 1)^{1/2} \tag{2.31}$$

The condition that convective instability has time to grow substantially before one wave period is given by $\sigma_{\max} > \Omega$. Using (2.31), (2.15) and (2.13), the critical amplitude for convective instability to develop is

$$A_{CV} = \frac{1}{2\pi}\cot\Theta(1 + \cos^2\Theta). \tag{2.32}$$

Hereafter, a wavepacket with amplitude $A > A_{CV}$ is said to satisfy the 'breaking condition'. Note that $A_{CV} \simeq 2A_{OT} \to \infty$ in the limit $\Theta \to 0$.

A third condition governing the stability of waves to overturning and breaking is based on a proposal by McIntyre (1973) and the analytic calculations by Grimshaw (1975*a*, *b*) for vertically bounded internal wave modes in a channel. The latter explicitly showed that the theory used to derive the weakly nonlinear dispersion relation (2.24) breaks down when there is a resonant interaction between the waves of vertical mode number m and horizontal wavenumber k with a long wave of mode number $2m$. The

interaction is unusual in that it involves a matching between the *group velocity* of the wavepacket and the phase speed of the long wave mode. Indeed, Grimshaw has shown that when the resonant interaction occurs the amplitude of the interaction is comparable with that of the wave itself, and the waves grow linearly in time if the horizontal extent of the wavepacket is sufficiently large.

These results may be extended to internal waves that are vertically unbounded, which corresponds to the limit of large vertical mode number m. In this limit, the long wave mode is just the wave-induced mean flow, and the resonant interaction describes the process of wave self-acceleration. Thus, provided the horizontal extent of a wavepacket is sufficiently large compared with the horizontal wavelength, instability due to self-acceleration will occur.

Whether owing to this resonant interaction waves will grow to such amplitude that they break cannot be assessed by a weakly nonlinear theory.

Nor does it seem that nonlinear stability theories can be applied. The nonlinear stability of some fluid flows may be assessed by way of Arnol'd's theorems (Arnol'd 1969) applied to the conservation laws determined from Hamiltonian fluid dynamics. This approach has been used successfully to provide sufficient conditions for stability of uniform, incompressible, inviscid flow (for example, see Shepherd 1990). The stability of stratified flows has been more difficult to assess in this way. In considering the limit from a multi-layer to continuously stratified model, Ripa (1991) has shown that the corresponding stability criterion describes only the stability of normal modes and not the subsequent nonlinear evolution. Ripa has concluded that the stability of continuously stratified flows probably cannot be assessed by conservation laws.

The approach here is to derive an explicit formula that predicts at what amplitude self-acceleration effects are non-negligible, and then to examine the fully nonlinear evolution of the waves. In § 5, the simulations indeed show that an initially statically stable wavepacket that is, nonetheless, of sufficiently large amplitude evolves nonlinearly: the waves interact with the wave-induced mean flow until they become statically unstable and break.

The critical amplitude at which waves interact resonantly with the mean flow is given by matching the predicted maximum value of the wave-induced mean flow, given by (2.18), with the horizontal group velocity of the waves, given by (2.16). Solving $A_M = c_{gx}$, and using (2.15) to write the condition in terms of the non-dimensional amplitude A, the critical amplitude is

$$A_{SA} = \frac{1}{2\pi\sqrt{2}} \sin 2\Theta. \tag{2.33}$$

Hereafter, the waves are said to satisfy the 'self-acceleration condition' if $A > A_{SA}$. The maximum value of the right-hand side of this inequality occurs for waves propagating at an angle $\Theta = 45^\circ$ to the vertical (that is, if $k_x = k_z$), in which case marginal stability occurs when $A_\xi = (1/2\pi\sqrt{2})\lambda_x \simeq 0.11\lambda_x$. Thus interactions between the waves and the wave-induced mean flow are expected to be relevant even if the amplitude of the initial wavepacket is an order of magnitude smaller than the horizontal wavelength. This fact provides *a posteriori* support for the assumption that linear theory can provide a useful estimate of the stability boundary, even though the instability itself ultimately occurs due to weakly nonlinear effects.

Figure 3 schematically illustrates the above-described domains of stability and instability. Based on the above arguments, only those waves with values of Θ and amplitudes, A, indicated by the hatched region are stable. The stability boundary is

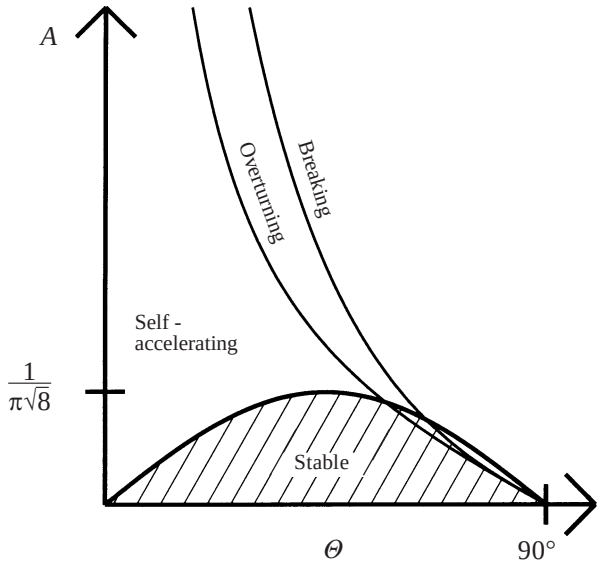

FIGURE 3. Schematic showing domains of stability and instability of internal waves as a function of Θ, the tilt of the phase lines with respect to the vertical, and the initial wavepacket amplitude A, the ratio of the maximum vertical displacement to the horizontal wavelength.

set by (2.33) for $\Theta \lesssim 65.5°$. Some of the calculated properties and critical amplitudes for internal wavepackets examined in detail here are listed in table 1.

Note that the marginal stability curve for the breaking condition lies well above the marginal stability curve for self-acceleration for non-hydrostatic waves (with $\Theta \lesssim 45°$). Thus if one considers a circumstance where a stable non-hydrostatic wavepacket propagating in the atmosphere gradually increases in amplitude (for example due to non-Boussinesq effects), then one should expect the wavepacket to become unstable due to self-acceleration before it is of sufficiently large amplitude to be unstable due to convective breaking.

As Appendix B demonstrates, instability due to self-acceleration does not occur for deep water waves because they reach breaking amplitudes before the wave-induced mean flow is comparable to the phase speed of the waves.

In the preceding discussion, dynamic instability has been ignored because the onset of dynamic and convective instability occurs for waves of approximately the same amplitude if their frequency is large and background rotation effects are negligible (Dunkerton 1989): the overturning condition and the dynamical instability condition are identical. For waves near inertial frequencies (with $\Theta \simeq 90°$), strong shear may drive the waves to become dynamically unstable through Kelvin–Helmholtz instability (Fritts & Rastogi 1985). Examination of these hydrostatic dynamics is beyond the scope of this work.

3. Model description

The propagation of internal waves is examined using a fully nonlinear numerical model that simulates fluid motion in two dimensions in a doubly periodic domain and in a periodic channel flow. The model has been employed recently to examine the propagation and reflection of internal waves in non-uniformly stratified, stationary flows (Sutherland 1996) and in uniformly stratified, shear flows (Sutherland 1999, 2000).

Wavepacket characteristics		Linear theory			
$\lvert k_z\rvert/k_x$	Θ (deg.)	$(c_{gx}, c_{gz})\dfrac{k_x}{N_0}$	A_{OT}	A_{CV}	A_{SA}
0.4	21.8	(0.128, 0.320)	0.40	0.74	0.078
2.5	68.2	(0.320, 0.128)	0.064	0.073	0.078

Wavepacket characteristics			Static stability		Wave-induced mean flow	
$\lvert k_z\rvert/k_x$	Θ (deg.)	A	$-\dfrac{A_{\Delta N^2}}{N_0^2}$	$\dfrac{\min\{\Delta N^2\}}{N_0^2}$	$A_M\dfrac{k_x}{N_0}$	$M_{\max}\dfrac{k_x}{N_0}$
0.4	21.8	0.0034	−0.009	−0.01	0.0003	0.00016
0.4	21.8	0.069	−0.17	−0.45	0.10	0.21
0.4	21.8	0.086	−0.21	−1.09	0.16	1.3
2.5	68.2	0.0086	−0.14	−0.13	0.004	0.0028
2.5	68.2	0.069	−1.08	−1.9	0.25	0.43
2.5	68.2	0.086	−1.35	−5.5	0.39	1.1

TABLE 1. Characteristics of internal wavepackets in simulations of horizontally periodic waves with wavenumber (k_x, k_z) and amplitude A. Θ is given implicitly by (2.13); $\boldsymbol{c}_g$ is the group velocity; the overturning, breaking and self-acceleration conditions are represented by critical amplitudes given by (2.29), (2.32) and (2.35), respectively; $A_{\Delta N^2}$ is given by (2.28) and A_M is given by (2.18); the minimum value of the ΔN^2 field up to time $t \simeq 16T$ and the wave-induced mean flow $M_{\max}$ at time $t \simeq 16T$ are determined from simulations.

The numerical model solves the discretized form of the equations (2.2) and (2.3). The basic-state fields are represented by the discrete Fourier coefficients of their horizontal structure and are sampled at equally spaced intervals in the vertical. Vertical derivatives are taken using a second-order finite difference scheme. The code is advanced in time using a second-order 'leap-frog' with an Euler backstep taken at regular intervals (Smyth & Peltier 1993; Sutherland & Peltier 1994).

Although it is desirable here to neglect diffusion effects, it is nonetheless necessary to include the diffusion-like terms $\mathscr{D}_\zeta$ and $\mathscr{D}_\xi$ in order to eliminate the growth of small-scale numerical noise. Typically, $\mathscr{D}_\zeta = \mathscr{D}\zeta$ and $\mathscr{D}_\xi = \mathscr{D}\xi$, where $\mathscr{D}$ is taken to be the product of an effective diffusion constant, $1/Re$, times a Laplacian diffusion operator acting only on horizontal scales smaller than the horizontal wavelength of the initial wavepacket. The effective Prandtl number is thus equal to 1. Here the Reynolds number $Re = 1000$ is used, based on the lengthscale $\lambda_x/2\pi$ and the timescale $T/2\pi$, where λ_x is the horizontal wavelength of the initial waves and T is the background buoyancy period, $T = 2\pi/N_0$.

This diffusion scheme has been employed to damp small-scale noise while allowing the initial wavepacket to evolve as if it were propagating in effectively inviscid fluid. However, in simulations in which waves convectively break, Re is nonetheless sufficiently small that the code remains numerically stable if run at high resolution. For comparison, simulations have also been performed with $\mathscr{D} \equiv (1/Re)\nabla^2$ acting on all wavelengths. In terms of Θ and N_0, the timescale of diffusion acting on the initial wavepacket is predicted to be $Re\cos^2\Theta/(2\pi N_0)$ (Sutherland 2000). Indeed, with $Re = 10\,000$, the amplitude and structure of non-hydrostatic wavepackets are found to be negligibly different over the duration of the simulation from those in simulations where the diffusion operator acts only on small scales.

The simulations are run between times $t = 0$ and $t = 100/N_0 \simeq 16T$, approximately 16 buoyancy periods. Time steps are taken at intervals of $0.0016T$ with an Euler backstep taken every 20 steps.

In simulations of doubly periodic waves, the boundary conditions are set to be both horizontally and vertically periodic, and the domain size is set to accommodate exactly one vertical and one horizontal wavelength of the initial wavepacket. The simulations have been run with resolutions of 32 by 32 and 64 by 64 points spanning the domain. (Thus, in the horizontal the discrete Fourier coefficients are cut off at wavenumbers above $32k_x$.)

In simulations of vertically compact wavepackets, the upper and lower boundaries are rigid with free-slip conditions. However, the vertical extent of the model domain is set to be sufficiently large that the waves are of negligibly small amplitude at the upper and lower boundaries over the duration of each simulation. Whether or not vertically bounded or vertically periodic boundary conditions are used is found to be irrelevant in these cases. Typically, the vertical extent of the domain ranges from $-40/k_x$ to $80/k_x$ ($\simeq -6.4\lambda_x$ to $12.7\lambda_x$) with the wavepacket centred initially at the origin. In simulations of horizontally periodic wavepackets, the horizontal extent of the domain is λ_x. Simulations have been run at resolutions ensuring that at least ten points span a single wavelength of the initial wavepacket. In most results reported here, the horizontal by vertical resolution is 64 by 1024 grid points.

In simulations of horizontally compact waves the horizontal extent of the domain is set to be much larger than the extent, σ_x, of the wavepacket itself. Typically $-16\lambda_x \leqslant x \leqslant 16\lambda_x$ for simulations with $\sigma_x = 10/k_x$. In simulations for which the horizontal extent of the domain is doubled, the evolution of the wavepacket is found to change negligibly. In order to perform a large number of these simulations, typically they are run at a horizontal by vertical resolution of 256 by 512. Resolution doubling tests have been performed for specific cases. No significant quantitative differences between the coarse and fine resolution simulations are found for the results reported herein.

4. Wave dispersion

In this section, the dispersion and weakly nonlinear stability of wavepackets is examined as a function of their amplitude and extent. The behaviour of small-amplitude waves in simulations is shown to be consistent with the predictions of linear theory. For waves of moderately large amplitude, however, nonlinear effects significantly alter the characteristics of the wavepacket. For very large-amplitude waves, breaking occurs due to wave self-acceleration. A detailed study of the last case is deferred to the next section.

4.1. *Horizontally periodic waves*

4.1.1. *Waves with vertical wavenumber* $k_z = -0.4k_x$

A range of simulations have been performed to examine the evolution of horizontally periodic, vertically compact internal waves as a function of their amplitude and wavenumber vector. Figure 4 shows the vertical displacement field and its associated power spectrum at time $t \simeq 16T$ for a small- and large-amplitude wavepacket with $k_z = -0.4k_x$. Figures 4(*a*) and 4(*b*) shows the results for a small-amplitude wavepacket with (non-dimensional) amplitude $A \simeq 0.0034$. The left-hand panel of figure 4(*b*) shows the normalized vertical displacement field, $\xi(x, z)/\lambda_x$, using the grey-scale indicated by the box in the top right corner. The scale ranges from -0.003 to

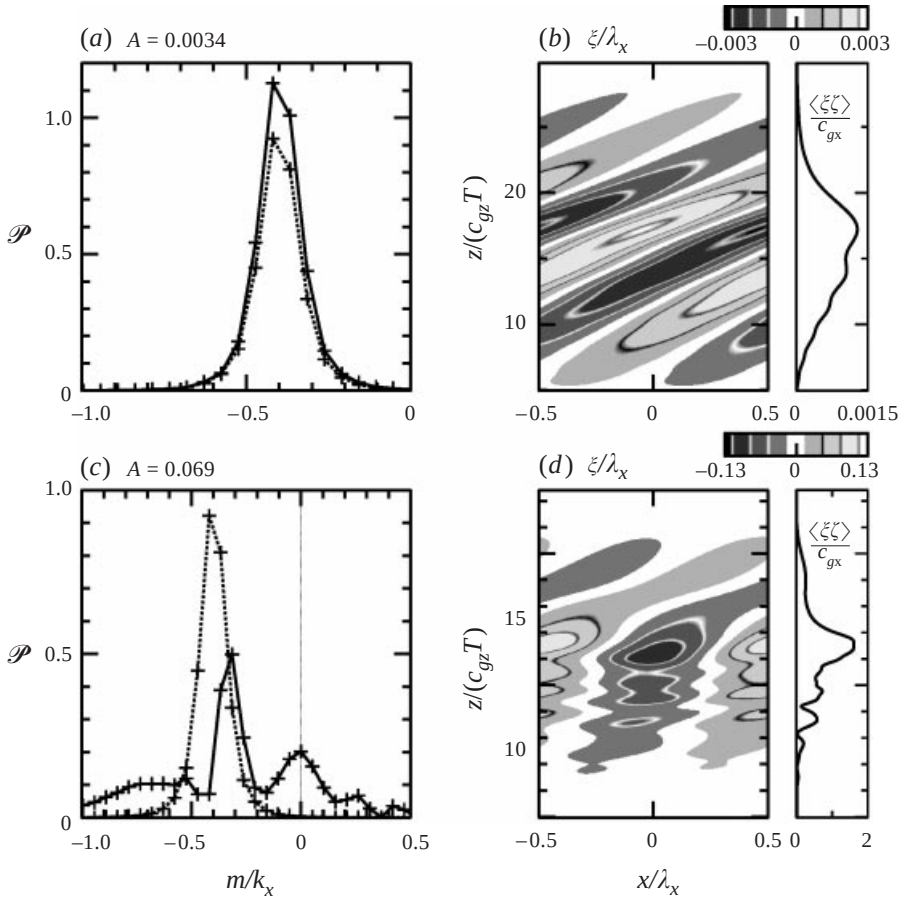

FIGURE 4. Comparison of (a,b) small- and (c,d) large-amplitude wavepacket structures with vertical wavenumber $k_z = -0.4k_x$ at time $t \simeq 16T$. (a) Power spectrum at $t \simeq 16T$ (solid line) compared with the power spectrum of the initial wavepacket (dashed line). Both are normalized by the peak power predicted by linear theory. (b) Left-hand panel shows the vertical displacement field normalized by the horizontal wavelength, and the right-hand panel shows the profile of $M(z)$, effectively a measure of the wave-induced mean flow, normalized by the predicted horizontal group velocity of the wavepacket, c_{gx}. Panels (c) and (d) correspond to (a) and (b), respectively, but for a wavepacket with amplitude initially 20 times larger.

0.003. The right-hand panel shows the corresponding vertical profile of the normalized wave-induced mean flow: $M(z)/c_{gx}$. The predicted peak value of $M(z)$ of the initial wavepacket is $A_M \simeq 2.5\times10^{-4}N_0/k_x$. At time $t \simeq 16T$, its peak value is approximately $1.6\times10^{-4}N_0/k_x$. These values are much smaller than the predicted horizontal group velocity of the wavepacket, $c_{gx} \simeq 0.128N_0/k_x$. Thus the effects of self-acceleration are not expected to be relevant in this case.

The nonlinear dispersion of the wavepacket is assessed by examining contours of the power spectra at time $t \simeq 16T$. Here the spectra are determined from the square of the discrete Fourier transform of the vertical displacement field which is normalized by the predicted peak value

$$\mathscr{P}_{\max} = 4\pi^2\left(A\frac{1}{k_x}\frac{\sigma_z}{L_z}\right)^2, \tag{4.1}$$

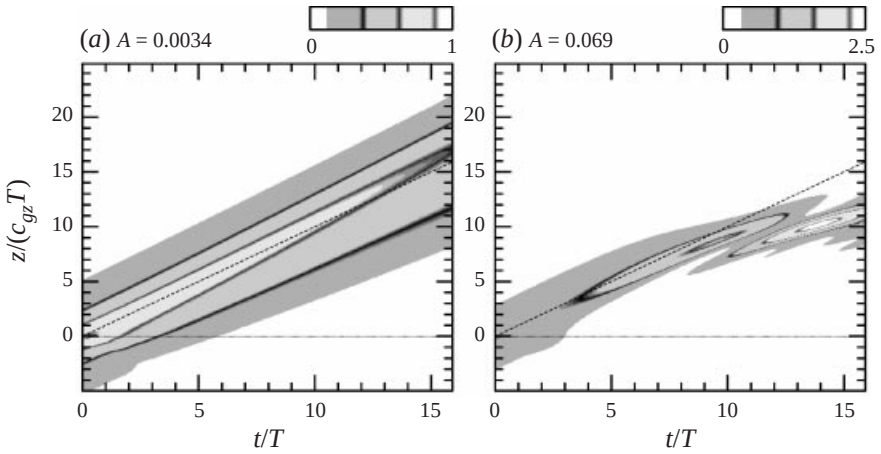

FIGURE 5. Horizontally averaged energy profile of (*a*) small-amplitude and (*b*) moderately large-amplitude internal wavepacket with $k_z = -0.4k_x$. The wavepacket is nonlinearly unstable to modulations of the vertical structure.

in which L_z is the vertical extent of the domain. Figure 4(*a*) shows the normalized power spectra as a function of the vertical wavenumber m. The spectrum at $t \simeq 16T$ is determined from the vertical displacement field and is compared with the initial spectrum (dashed curve). Throughout the wavepacket evolution, the spectrum of the waves remains peaked at $m = -0.4k_x$, close to the initial vertical wavenumber. The discrepancy between the initial and final structure of the power spectrum occurs primarily because the vertical extent of the initial wavepacket is comparable to the vertical wavelength.

These diagnostics confirm that the small-amplitude wavepacket undergoes negligible dispersion and that the dynamics governing the wavepacket evolution are numerically well resolved.

The small-amplitude simulation results are compared with those of a large-amplitude wavepacket with the same wavenumber as that discussed above, but with $A \simeq 0.069$. Figure 4(*c*) shows that the spectrum of the large-amplitude waves is spread out over a broader range of m. Thus the waves are of sufficiently large amplitude that weakly nonlinear dispersive effects are non-negligible. The structure of the wavepacket at time $t \simeq 16T$ is shown in figure 4(*d*). It is immediately apparent that the wavepacket has not propagated as far vertically as its small-amplitude counterpart. The vertical extent of the wavepacket is smaller and the lines of constant phase tilt more closely to the vertical near the centre.

The right-hand panel of figure 4(*d*) shows a plot of the wave-induced mean flow $M(z)$ normalized by the horizontal group velocity at time $t \simeq 16T$. Because the peak value of the wave-induced mean flow is approximately 50% larger than the horizontal group velocity, the effects of self-acceleration are non-negligible in this case. The peak value, $M_{\max}$ of $M(z)$ is compared with the initial value predicted by linear theory in table 1.

The effect of weakly nonlinear dispersion upon the envelope of the wavepacket is demonstrated in figure 5, which shows vertical time series of the horizontally averaged energy corresponding to the waves. In both diagrams the energy is normalized by the maximum energy predicted by linear theory: $2|\boldsymbol{k}|^2 {A_0}^2$. Figure 5(*a*) shows that the small-amplitude wavepacket propagates vertically upward at approximately constant

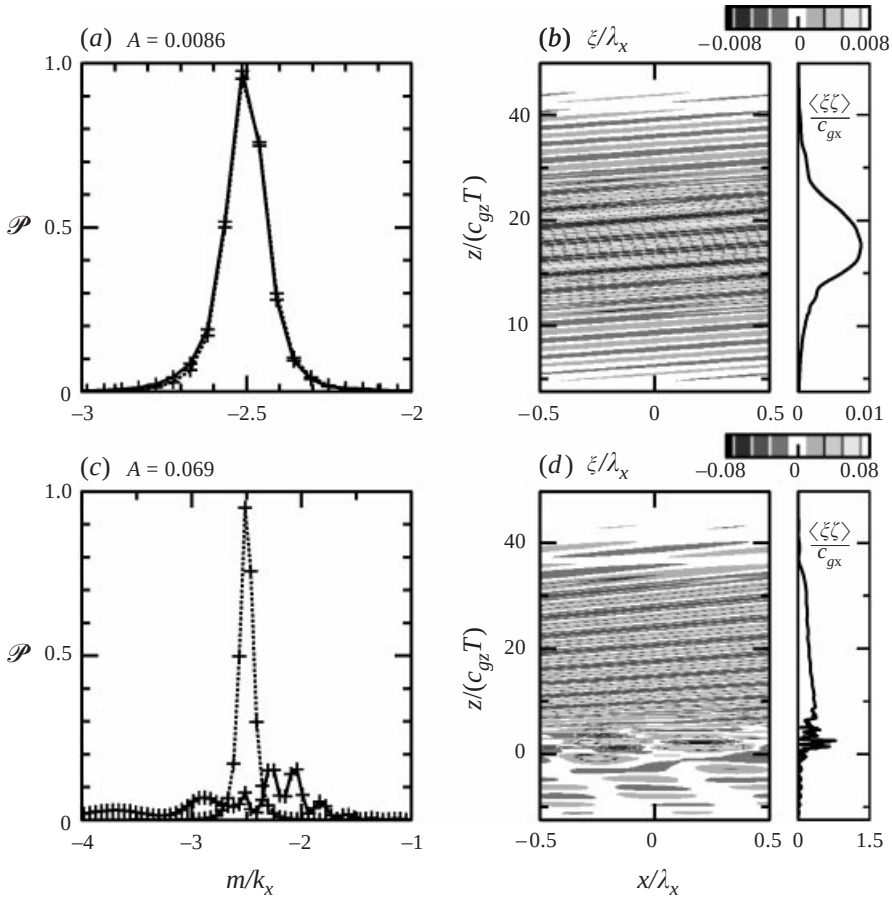

FIGURE 6. As in figure 4 but for small- and large-amplitude wavepackets with vertical wavenumber $k_z = -2.5k_x$.

speed equal to the vertical group velocity (indicated by the superimposed diagonal dashed line). Figure 5(*b*) shows that the large-amplitude wavepacket initially increases in amplitude. This behaviour is consistent with weakly nonlinear theory, as expressed by (2.23), which predicts that the waves should be unstable due to finite-amplitude modulations. The wavepacket amplitude does not grow indefinitely but, consistent with the Fermi–Pasta–Ulam recurrence phenomenon (Fermi *et al.* 1974), the envelope first peaks in amplitude at time $t \simeq 9.5T$, weakens, then peaks again at time $t \simeq 14T$.

The wavepacket as a whole propagates vertically at a substantially slower speed than the group velocity predicted by linear theory.

4.1.2. *Waves with vertical wavenumber* $k_z = -2.5k_x$

Weakly nonlinear effects are significantly different for wavepackets with small vertical wavelength compared with the horizontal wavelength, as anticipated from (2.23). As in figure 4, figure 6 shows the structure at time $t \simeq 16T$ of a small-amplitude wavepacket (with $A = 0.0086$) and a large-amplitude wavepacket (with $A = 0.069$) in which the vertical wavenumber is $k_z = -2.5k_x$.

Figure 6(*a*) shows that there is negligible difference between the initial and final power spectrum of the waves. Both are sharply peaked about $m = -2.5k_x$, with

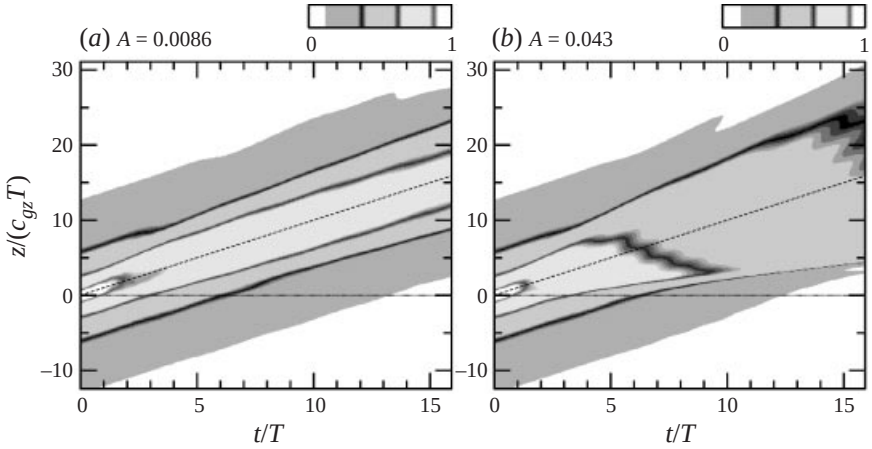

FIGURE 7. Horizontally averaged energy profile of (*a*) small-amplitude and (*b*) moderately large-amplitude internal wavepacket with $k_z = -2.5k_x$. The wavepacket is stable to weakly nonlinear modulations of the vertical structure.

maximum (normalized) value close to unity, as expected from linear theory. The wavepacket at time $t \simeq 16T$, shown in figure 6(*b*), has undergone only weak dispersion with a well-defined peak amplitude. The peak value of $M(z)$, shown in the right-hand panel of figure 6(*b*), is less than 1% of the horizontal group velocity predicted by linear theory ($c_{gx} \simeq 0.32N_0/k_x$) so the effects of self-acceleration are negligible.

In the large-amplitude case, however, the spectrum is broadly distributed over a wide range of vertical wavenumbers with multiple, but relatively small peaks (figure 6*c*). From the left-hand panel of figure 6(*d*), it is apparent that the waves tilt more closely to the vertical near the leading edge of the wavepacket. This effect was also observed by Fritts & Dunkerton (1984) in their study of saturation and self-acceleration. In their simulations, the waves were forced at a relatively low frequency so that $\Theta \simeq 77°$.

The structure of the plot of $M(z)$, shown in the right-hand panel, is qualitatively very different from its counterpart in figure 4 where $k_z = -0.4k_x$. Rather than being strongly peaked over a small vertical distance, here $M(z)$ is approximately uniform over a wide vertical range, but exhibits large-valued spikes near the trailing edge of the wavepacket. The peak value of $M(z)$ is comparable to the horizontal group velocity predicted from linear theory.

The effect of finite-amplitude modulations on the wavepacket are demonstrated in figure 7. As in figure 5 this shows the vertical time series of the horizontally averaged energy field. The field is normalized by the maximum value predicted by linear theory. For small-amplitude waves, the wavepacket moves vertically upward at the same speed as the predicted vertical group velocity. For large-amplitude waves, the envelope of the wavepacket spreads out and the amplitude decreases in time. These results are consistent with (2.23) which predicts that this wavepacket is stable to finite-amplitude modulations. Weakly nonlinear theory predicts that the wavepacket should subdivide into two groups that propagate vertically at speeds respectively greater than and less than c_{gz}, the vertical group velocity of linear theory. Consistent with this theory, the average vertical speed of the wavepacket is observed to be close to c_{gz}.

The results in this section serve to demonstrate qualitatively that finite-amplitude effects are important when the amplitude of the waves is sufficiently large that the

wave-induced mean flow is comparable with the horizontal group velocity of the waves. Furthermore, they emphasize that finite-amplitude effects are significant even when the amplitude itself is seemingly small: in the simulation discussed above with $A = 0.069$ and $k_z = -0.4k_x$, the amplitude of the initial wavepacket is well below the amplitude, $A_{OT} \simeq 0.40$, of overturning of the waves, but only moderately below the critical amplitude for self-acceleration A_{SA} (see table 1).

4.2. *Horizontally compact waves*

The dispersion of large-amplitude wavepackets that are horizontally as well as vertically compact is significantly different from that of horizontally periodic internal waves. This is anticipated for two reasons. First, weakly nonlinear theory predicts that finite-amplitude wavepackets are unstable to horizontal modulations if Θ is sufficiently large, as given explicitly by (2.25) for internal waves confined vertically in a channel (Grimshaw 1977). In contrast, horizontally periodic, vertically compact wavepackets are predicted to be stable for such large values of Θ (e.g. see (2.23)).

Second, it follows from symmetry that horizontally periodic waves satisfy the conservation of pseudomomentum. This conservation law does not hold for waves that are spatially inhomogeneous in the horizontal (Shepherd 1990). This symmetry argument is identical to noting that a horizontally compact wavepacket cannot induce a mean flow over the entire horizontal extent of the domain: there can be no wave-induced mean flow where the amplitude of the waves is negligibly small. Nonetheless, if a horizontally compact wavepacket contains many wavelengths, it is reasonable to suppose that the waves will induce a mean flow over the horizontal extent of the wavepacket. If the waves are of sufficiently large amplitude that the wave-induced mean flow is comparable with the horizontal group velocity, then the horizontal structure of the wavepacket will be significantly altered by the effects of self-acceleration.

The influence of the wave-induced mean flow upon a horizontally compact wavepacket is diagnosed by calculating the field $M(x, z)$ defined by (2.19). The effects of self-acceleration are expected to be significant over regions of the wavepacket where $M(x, z) \gtrsim c_{gx}$.

4.2.1. *Waves with vertical wavenumber* $k_z = -0.4k_x$

Figure 8 shows the two-dimensional power spectra and wave structures at time $t \simeq 16T$ of a small- and large-amplitude wavepacket given by (2.12) with $k_z = -0.4k_x$ and $\sigma_x = \sigma_z = 10/k_x$.

For a simulation of a small-amplitude wavepacket with $A \simeq 0.0034$, the computed power spectrum of the waves at time $t \simeq 16T$ is shown in figure 8(*a*). The field is normalized by

$$\mathscr{P}_{\max} = 8\pi^2 \left(A \frac{1}{k_x} \frac{\sigma_x \sigma_z}{L_x L_z} \right)^2, \tag{4.2}$$

the predicted peak power of the discrete two-dimensional Fourier transform of the initial wavepacket. The plot illustrates that the peak value is negligibly different from its initial value and is centred near its initial wavenumber.

The corresponding vertical displacement field is shown in figure 8(*b*). The magnitude of the field is illustrated by the grey-scale indicated in the upper right-hand box. The black lines superimposed on the vertical displacement field are contours of $M(x, z)/c_{gx}$ shown in intervals of 0.0003. Its maximum value is approximately 0.001. Therefore, the effects of self-acceleration everywhere over the wavepacket are negligible. Indeed,

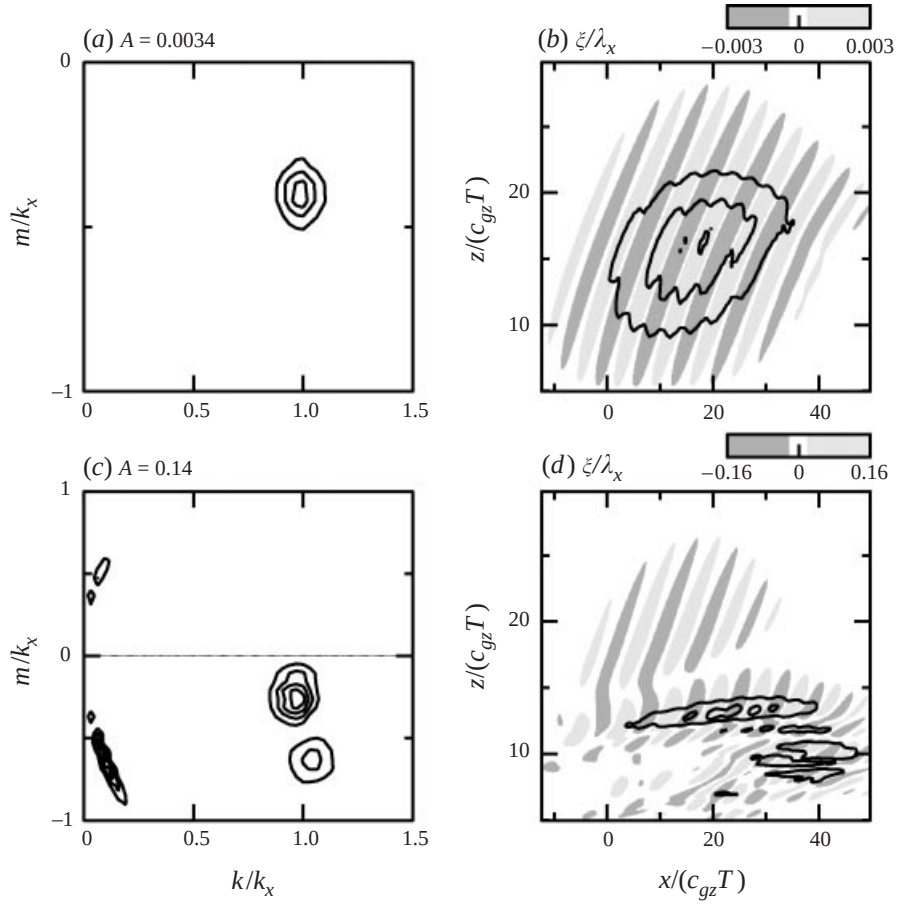

FIGURE 8. Comparison of (a, b) small- and (c, d) large-amplitude horizontally compact wavepackets with vertical wavenumber $k_z = -0.4k_x$ at time $t = 16T$. The wavepacket extent is given by $\sigma_z = \sigma_x = 10/k_x$. (a) Contours of the two-dimensional power spectrum normalized by the peak power predicted by linear theory. Contours are shown by intervals of 0.3. (b) The grey-scale shows values of the normalized vertical displacement field, $\xi(x, z)/\lambda_x$, and superimposed on it are contours of $M(x, z)$ normalized by c_{gx}, shown by intervals of 0.0003. Panels (c) and (d) correspond to (a) and (b), respectively, but for a wavepacket with amplitude initially 40 times larger. In (c) contours of the normalized power spectrum are shown by intervals of 0.05, and in (d) contours of the normalized $M(x, z)$ field are shown by intervals of 1.

the centre of the wavepacket is close to the position expected on the basis of linear theory at time $t \simeq 16T$: $(x, z) \simeq (16c_{gx}T, 16c_{gz}T)$.

By contrast, a large-amplitude wavepacket undergoes significant vertical and horizontal dispersion due to nonlinear effects. Figure 8(c) shows the power spectrum of the waves at time $t \simeq 16T$ for a simulation with $A = 0.137$. There are four distinct peaks in the spectrum. The strongest peak occurs near wavenumber $(k, m) = (0.96, -0.31)k_x$, and a peak almost as strong occurs near $(0.09, -0.63)k_x$. The strength and position of these peaks do not change in simulations performed with domains four times as large and in simulations with quadruple the resolution. Peaks of smaller magnitude occur near $(1.02, -0.61)k_x$ and $(0.06, 0.51)k_x$. Thus, like the case of horizontally periodic waves, due to nonlinear effects the spectrum exhibits peaks near $k = k_x$ but with smaller and larger vertical wavenumbers than $k_z = -0.4k_x$. Unlike the case of hor-

izontally periodic waves, however, the vertical displacement field exhibits significant power at small horizontal wavenumbers $k \simeq 0.1k_x$. Its value is set by the horizontal extent of the wavepacket $\sigma_x = 10/k_x$. Indeed, in simulations of wavepackets of larger horizontal extent, the peak power for small horizontal wavenumbers occurs at successively smaller values of k. These values of k decrease approximately in inverse proportion to σ_x. A large spectral peak occurs at small horizontal wavenumbers because of the interaction between waves of horizontal wavenumber k_x and the wave-induced mean flow acting over the extent of the wavepacket.

Figure 8(d) shows the corresponding vertical displacement field and contours of $\langle M(x,z)\rangle_{\lambda_x}$. At time $t \simeq 16T$ the wavepacket has developed a complex structure as a result of interactions between the waves and the wave-induced mean flow. The initial wavepacket has subdivided into multiple wavepackets, and the $\langle M(x,z)\rangle_{\lambda_x}$ field exhibits many peaks with values larger than c_{gx}. Thus, as a result of nonlinear dispersion effects, the initial wavepacket subdivides into multiple wavepackets some of which propagate at speeds approximately twice as large as the horizontal group velocity predicted by linear theory: under the effects of self-acceleration, the wavepacket is advected at speeds greater than c_{gx} by the wave-induced mean flow.

4.2.2. *Waves with vertical wavenumber* $k_z = -2.5k_x$

For a wavepacket composed of waves with Θ large, it is found that the mechanism of nonlinear dispersion acts much more weakly, even for waves with amplitudes only moderately smaller than that required for instability and breaking.

The results of simulations of a horizontally compact wavepacket with $k_z = -2.5k_x$ and $\sigma_x = \sigma_z = 10/k_x$ are shown in figure 9. Figure 9(a) shows the normalized power spectrum of a small-amplitude wavepacket with $A = 0.0086$ after it has propagated from the origin for time $t \simeq 16T$. As expected for a quasi-plane small-amplitude wavepacket, the spectrum is sharply peaked near $(k,m) = (k_x, -2.5k_x)$ with value close to unity. Figure 9(b) shows the corresponding vertical displacement field with superimposed contours of $M(x,z)/c_{gx}$. The wavepacket is centred near $(x,z) \simeq (16c_{gx}T, 16c_{gz}T)$ as expected from linear theory. The wave-induced mean flow is everywhere much less than the horizontal group velocity, so the effects of self-acceleration are negligible.

Figure 9(c) shows the normalized power spectrum at time $t \simeq 16T$ of a large-amplitude wavepacket with $A = 0.086$. Unlike the case with $k_z = -0.4k_x$, here the spectrum of the horizontally compact waves is negligibly different from that of the small-amplitude waves as seen by comparing figures 9(a) and 9(c).

Nonetheless, nonlinear effects have significantly altered the structure of the wavepacket as shown in figure 9(d). Similar to the corresponding simulations of large-amplitude horizontally periodic waves with $k_z = -2.5k_x$, the waves are quasi-periodic along their leading edge but exhibit irregular behaviour along the trailing left-hand-side edge of the wavepacket. Only in this region is the $M(x,z)$ field significant. The inset to figure 9(d) shows the contours of $M(x,z)/c_{gx}$ superimposed on a close-up of the vertical displacement field for $7 \leqslant x/(c_{gx}T) \leqslant 14$ and $0 \leqslant z/(c_{gz}T) \leqslant 3$.

In simulations of wavepackets with moderately larger amplitude than this, the waves become convectively unstable before time $t \simeq 16T$ in the trailing region of the wavepacket.

Thus, in comparison with the results for horizontally periodic waves, large-amplitude horizontally compact wavepackets excite long horizontal wavelengths if they are non-hydrostatic ($|\Theta|$ small), but the dispersion of the waves is inhibited if $|\Theta| \simeq 90^\circ$. In the former case, the peak power of a large-amplitude horizontally com-

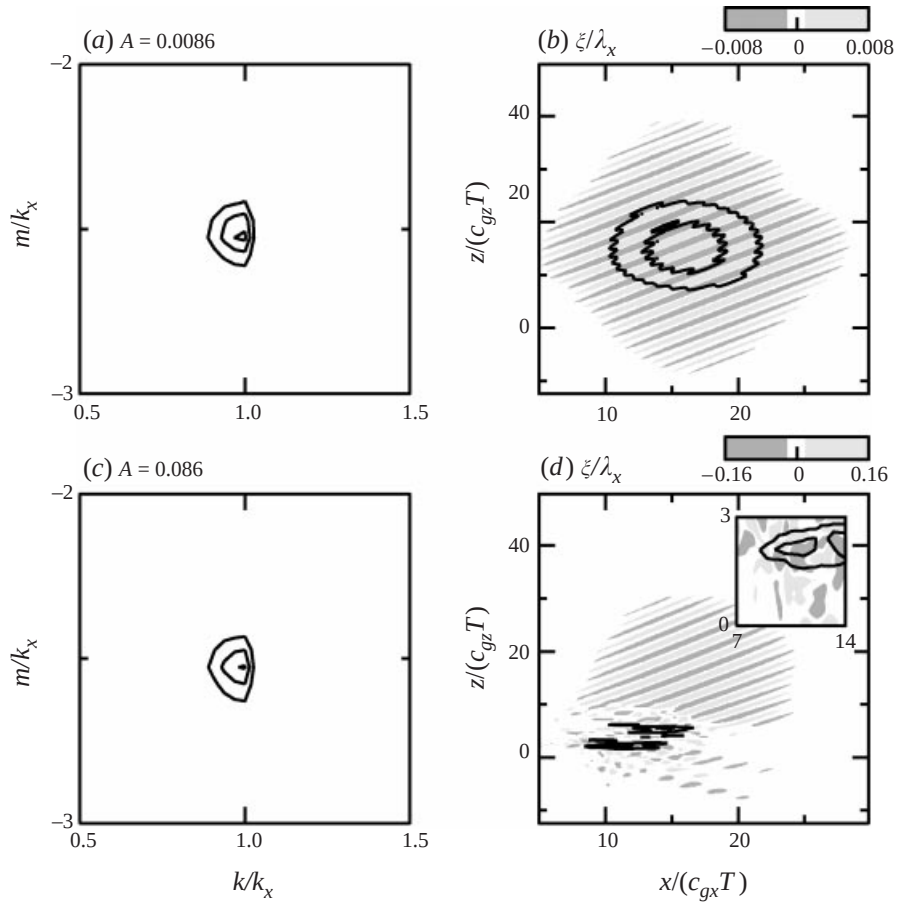

FIGURE 9. As figure 8 but for a wavepacket with $k_z = -2.5k_x$. In (*a*), the contours of the normalized power spectrum of the small-amplitude wavepacket are shown by intervals of 0.3. In (*b*), the contours of the normalized $M(x, z)$ field are shown by intervals of 0.002. Diagrams (*c*) and (*d*) show the results if the amplitude of the initial wavepacket is 10 times larger. In (*c*) contours of the normalized power spectrum are shown by intervals of 0.2, and in (*d*) contours of the normalized $M(x, z)$ field are shown by intervals of 2. The inset shows a close-up of a region in the wave field where $M(x, z) \gg c_{gx}$. The grey scale and contour interval are the same.

pact wavepacket decreases over time to a greater extent than horizontally periodic waves.

5. Wave breaking

It is generally accepted that an internal wave will break, adding momentum to the mean flow, if its amplitude is so large that it is overturning (e.g. Gill 1982, § 8.10). For a quasi-plane wavepacket, the critical amplitude at which overturning occurs is given by (2.29), where, from (2.13), $\Theta = \cos^{-1}(\Omega/N_0)$. Here it is demonstrated by way of numerical simulations that this value generally underestimates the critical amplitude at which the wave actually overturns and convectively breaks. A more accurate prediction of the critical amplitude for convective breaking is given by (2.32).

The numerical simulations also show that a wavepacket with amplitude initially well below that of a breaking wave may nonetheless evolve so that it eventually overturns. For horizontally periodic waves, the critical amplitude at which such

breaking occurs is shown to be comparable with the predicted critical amplitude given by the 'self-acceleration' condition (2.33).

Below it is shown that this mechanism for breaking is different from breaking due to parametric instability.

5.1. *Parametric instability and self-acceleration*

Analytic theories and numerically computed stability calculations have shown that, even at infinitesimally small amplitudes, plane periodic internal waves are unstable to parametric instability whereby the superharmonic waves draw energy from the fundamental waves until they grow to such amplitude that they break (Mied 1976; Drazin 1977; Klostermeyer 1991; Lombard & Riley 1996). This result assumes the waves are perfectly monochromatic, and hence have constant amplitude everywhere, as shown in figure 1(*a*). One might assume the results could be extended to quasi-plane waves, such as those shown in figures 1(*b*) and 1(*c*). However, it is shown here that interactions between the waves and the wave-induced mean flow dominate the evolution and stability of compact wavepackets.

Wave–wave and wave–mean flow interactions are diagnosed by continually calculating the spectrally decomposed transfer rates of energy from one horizontal wavenumber to another during a simulation (Herring *et al.* 1974; Smyth & Peltier 1992; Sutherland & Peltier 1994). The details of this calculation are given in Appendix C. Specifically, the rate of energy transport between the mean flow, the fundamental waves (with horizontal wavenumber k_x) and the superharmonics (with horizontal wavenumber $2k_x$) is determined from a spectral decomposition of the energy equation using (C 9), (C 10) and (C 11). At early times in all the studies discussed here it is found that energy is exchanged between these three modes alone. Thus parametric wave excitation may be diagnosed simply by examining the transfer of energy into modes with horizontal wavenumber $2k_x$.

Figure 10 shows the spectral energy transfer rates between waves and the mean flow computed up to time $t \simeq 16T$ in simulations of small- and large-amplitude wavepackets which are doubly periodic (monochromatic) and horizontally periodic but vertically compact. In all four cases $k_z = -0.4k_x$. The streamfunction amplitude envelope of the doubly periodic waves is given initially by (2.10), and the evolution equations (2.2) and (2.3) are solved in a domain with vertically and horizontally periodic boundary conditions.

The rate of energy transfer from waves to the mean flow, T_{W0}, is plotted over time by a solid line. As is typical for all horizontally periodic wavepacket evolution simulations that have been examined, T_{W0} is equal in magnitude but opposite in sign to the energy transfer rate from the mean flow to waves with horizontal wavenumber k_x, that is $T_{W0} \simeq -T_{01}$ in which T_{01} is given by (C 11), and is plotted over time by a long-dashed line in figure 10. The energy transfer rate from waves to the fundamental waves, T_{W1}, is plotted over time by a short-dashed line, and the energy transfer rate from waves to the superharmonic waves, T_{W2}, is plotted over time by a dotted line. Again, as is typically observed, $T_{W1} = -T_{W2}$: energy is exchanged between waves primarily between the fundamental and the first superharmonic. In all four simulations clearly energy is exchanged between the mean flow and the fundamental waves through interactions distinct from the exchange of energy between the fundamental waves and the superharmonic with horizontal wavenumber $2k_x$.

For relatively small-amplitude doubly periodic waves with $A = 0.017$ (figure 10*a*), energy is simultaneously transferred from the mean flow to the fundamental while the fundamental waves also draw energy from the superharmonic waves. In both

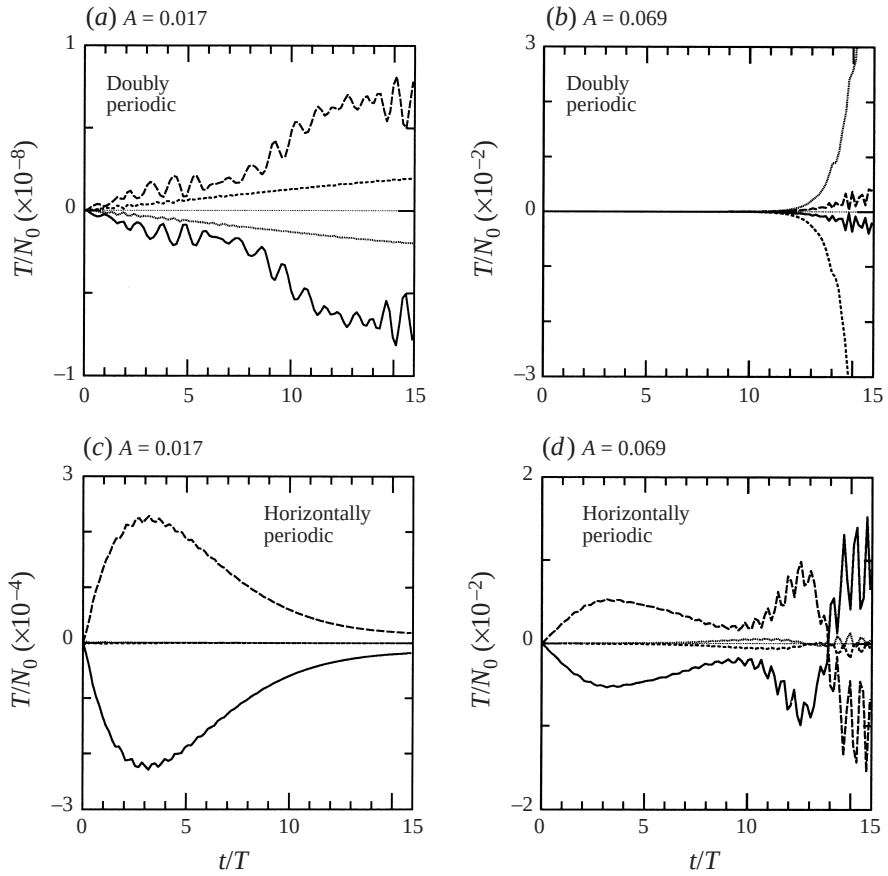

FIGURE 10. Comparison between doubly periodic and horizontally periodic, vertically compact wavepackets of energy transfers between waves and the mean flow for waves with $k_z = -0.4k_x$. For doubly periodic waves the results are shown for simulations of wavepackets with amplitude (*a*) $A = 0.017$ and (*b*) $A = 0.069$. Corresponding simulation results for horizontally periodic, vertically compact wavepackets are shown in (*c*) and (*d*), respectively. In each diagram, the energy transfer rates are shown from waves to the mean flow (solid line), from the mean flow to waves with horizontal wavenumber k_x (long-dashed line), from all waves to waves with horizontal wavenumber k_x (short-dashed line), and from all waves to waves with horizontal wavenumber $2k_x$ (dotted line).

instances, the energy transfer rates are less than 10^{-8} indicating that the growth of instabilities due to parametric resonance remains small over the duration of this simulation.

Significant growth of the superharmonic due to parametric resonance is observed, however, in simulations of doubly periodic waves with larger amplitude. As shown in figure 10(*b*), after time $t \simeq 12T$, significant energy is extracted from the fundamental by superharmonic waves (short-dashed and dotted lines). The energy extraction rate continues to increase exponentially until the waves overturn. Note that although the fundamental waves continue to extract energy from the mean flow (solid and long-dashed lines), this exchange is negligible compared with the wave–wave interactions.

For a doubly periodic wavepacket, the wave-induced mean flow (like the wavepacket envelope) is vertically uniform. However, for a vertically compact, horizontally periodic wavepacket, the wave-induced mean flow is large near the centre of the wavepacket and neglible where the amplitude of the waves is negligibly small on

either flank of the wavepacket. Therefore, as the wavepacket moves upward, the mean flow is accelerated on the upper flank of the wavepacket and it is decelerated on the lower flank. Owing to such interactions one expects that the energy transfers between waves and the mean flow will be greater for a vertically compact wavepacket.

Indeed, as shown for a small-amplitude vertically compact wavepacket simulation in figure 10(*c*), the fundamental waves extract energy from the mean flow at a rate four orders of magnitude greater than in the doubly periodic case. The mean-flow energy extraction rate is greatest at time $t \simeq 3T$. The exchange of energy between the fundamental and superharmonics is negligibly small over the duration of the simulation.

In a simulation of a vertically compact wavepacket with larger amplitude, $A = 0.069$, the mean flow is found to extract energy from the fundamental at times $t > 14T$, as shown in figure 10(*d*). Throughout this simulation, energy is also extracted from the fundamental by the superharmonics, but the exchange rate is small compared with the interactions between the waves and the wave-induced mean flow.

The energy exchange between doubly periodic and vertically compact waves is also computed for wavepackets with $k_z = -2.5k_x$, and is shown in figure 11. In both small- and large-amplitude doubly periodic wave simulations the fundamental waves exchange energy with the mean flow at a rate that varies with frequency comparable with N_0. The exchange of energy between the waves and the superharmonics is of comparable magnitude but varies approximately with frequency $2N_0$.

As in the case with $k_z = -0.4k_x$, figures 11(*c*) and 11(*d*) show that the dynamics of the wavepacket evolution are dominated by the exchange of energy between the fundamental and the wave-induced mean flow throughout the simulations. Referring to table 1, the critical amplitude for overturning waves with $k_z = -2.5k_x$ is 0.073. Thus, for the case shown in figure 11(*d*), the waves are large amplitude in the sense that the maximum vertical displacement is more than half that of overturning waves.

On the basis of these analyses, it is concluded that interactions between the waves and the wave-induced mean flow dominates over wave–wave interactions when the waves are vertically compact.

5.2. *Overturning and breaking*

Here the mechanism of wave breaking is examined in detail. As argued in § 3, one expects breaking to occur when the waves overturn and the timescale for the growth of convective instability is less than the order of the wave period.

However, as the simulations have shown, the structure of a finite-amplitude wavepacket is modified significantly as it evolves. Even if the initial amplitude of the wavepacket is well below that required for overturning, the wavepacket may evolve in such a way that it eventually overturns.

To demonstrate this, the minimum value of the ΔN^2 field everywhere in space is determined over time during a simulation. It is found that this minimum value does not vary greatly if the waves are of such small amplitude that $|\min\{\Delta N^2\}| \ll N_0^2$. However, if $|\min\{\Delta N^2\}| \gtrsim 2N_0^2$, the minimum value grows rapidly in magnitude due to the onset and growth of convective instabilities.

Figure 12 shows the time evolution of $\min\{\Delta N^2\}/N_0^2$ in simulations of horizontally periodic waves with (*a*) $k_z = -0.4k_x$ and (*b*) $k_z = -2.5k_x$. In figure 12(*a*), the values are plotted for waves with amplitude $A = 0.068$ (solid line), 0.085 (dotted line), and 0.10 (dashed line).

Three simulations at different resolutions are run for each value of k_z and A. The light curves show the results of a low-resolution simulation ($\Delta z \simeq 0.23/k_x$), medium-

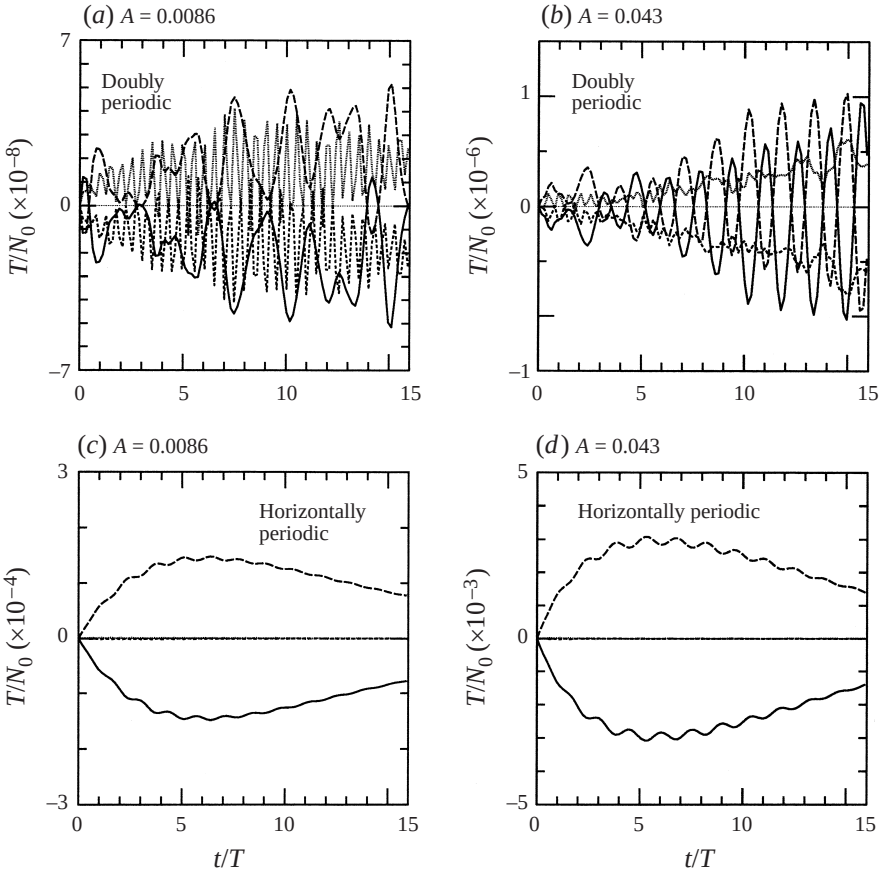

FIGURE 11. As in figure 10 but for waves with $k_z = -2.5k_x$. Each panel shows energy transfer rates from waves to the mean flow (solid line), from the mean flow to waves with horizontal wavenumber k_x (long-dashed line), from all waves to waves with horizontal wavenumber k_x (short-dashed line), and from all waves to waves with horizontal wavenumber $2k_x$ (dotted line).

weight curves show the results of standard simulations ($\Delta z \simeq 0.12/k_x$), and heavy curves show the results of high-resolution simulations ($\Delta z \simeq 0.06/k_x$), where Δz is the vertical spacing between grid points. Comparison between these curves shows that there is neglible difference between the results of standard and high-resolution simulations if $\min\{\Delta N^2\} > -N_0^2$. The evolution of breaking waves differs depending on the resolution, as one might expect since convective instability results in the rapid growth of small scales. Because convective breaking is a fully three-dimensional phenomenon, it would be a fruitless exercise to attempt to resolve small convection scales in a two-dimensional simulation. Nonetheless, the results show that the model accurately predicts at what time the onset of breaking occurs, if it occurs at all.

For the simulation with $k_z = -0.4k_x$ and $A = 0.069$, $\min\{\Delta N^2\}$ decreases gradually from its initial value of $-0.17N_0^2$ to a minimum value of $-0.57N_0^2$, before increasing again. If $A = 0.086$, $\min\{\Delta N^2\}$ is initially $-0.21N_0^2$, but it decreases to values close to $-N_0^2$ at time $t \simeq 8T$. After this time $\min\{\Delta N^2\}$ fluctuates to a greater extent and is as low as $-N_0^2$ at $t \simeq 16T$. In the large-amplitude case with $A = 0.10$, $\min\{\Delta N^2\}$ decreases from its initial value of $-0.25N_0^2$ to $-N_0^2$ after time $t \simeq 7T$.

While higher spatial and temporal resolution simulations could be run to examine

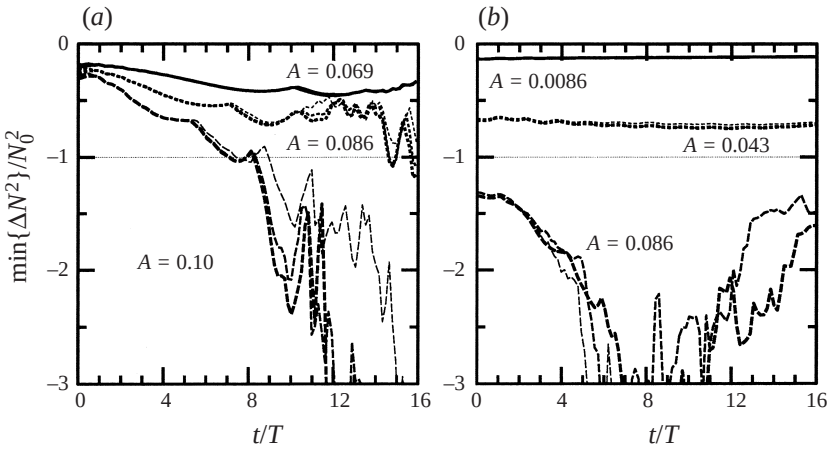

FIGURE 12. Plots over time of the minimum value of the ΔN^2 field normalized by N_0^2 for horizontally periodic wavepackets of different amplitudes (as indicated on plots), and vertical wavenumber (*a*) $k_z = -0.4k_x$ and (*b*) $k_z = -2.5k_x$. Light, medium and heavy curves correspond to low-, standard-, and high-resolution simulations, respectively (see text). The horizontal dotted line in both figures indicates the critical value of ΔN^2 when overturning occurs.

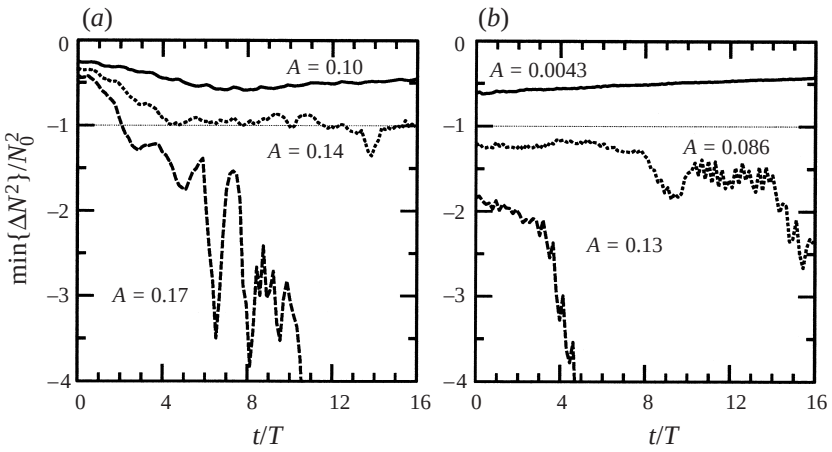

FIGURE 13. As in figure 12 but for horizontally compact wavepackets with $\sigma_x = 10/k_x$.

the convective dynamics in more detail, because the flows examined here are restricted to two dimensions, such an analysis would be unrealistic. It is sufficient here to remark that for waves of sufficiently large amplitude convective mixing does occur.

The stability of wavepackets with relatively small vertical wavelength is examined in figure 12(*b*), which shows the time evolution of $\min\{\Delta N^2\}/N_0^2$ in simulations with $k_z = -2.5k_x$. Values are plotted for waves with amplitude $A = 0.0086$ (solid line), 0.043 (dotted line), and 0.086 (dashed line). Unlike the case with $k_z = -0.4k_x$, here $\min\{\Delta N^2\}$ increases in time from its initial value when the initial amplitude is small. In the case where $A = 0.086$, $\min\{\Delta N^2\}$ is less than $-N_0^2$ initially. After about two buoyancy periods $\min\{\Delta N^2\}$ decreases rapidly in time.

The time evolution of $\min\{\Delta N^2\}/N_0^2$ is shown in figure 13 for a range of simulations of horizontally compact wavepackets. The results are similar to those for horizontally periodic waves. In simulations with $k_z = -0.4k_x$, figure 13(*a*), the value of $\min\{\Delta N^2\}$

A	$\min\{\Delta N^2\}/N_0^2\big\vert_{t=T}$	$\min\{\Delta N^2\}/N_0^2\big\vert_{t=4T}$	σT
0.034	−0.086	−0.090	0.016
0.052	−0.132	−0.158	0.066
0.069	−0.181	−0.271	0.166
0.086	−0.235	−0.448	0.302
0.10	−0.292	−0.647	0.405

TABLE 2. Values of $\min\{\Delta N^2\}/N_0^2$ determined at times $t = T$ and $t = 4T$ in simulations of horizontally periodic/vertically compact wavepackets with $k_z = -0.4k_x$ and a range of amplitudes A. The wave amplitude growth rate, σ, is estimated from these data using (5.1).

decreases over time initially and becomes approximately constant for amplitudes smaller than $A = 0.14$. When $A = 0.17$, however, $\min\{\Delta N^2\}$ decreases to values less than $-N_0^2$ at time $t \simeq 2T$. Afterward, the plot exhibits large fluctuations until after $t \simeq 11.6T$ when energy is rapidly deposited to small scales as a result of convective overturning. Figure 13(*b*) shows that when $k_z = -2.5k_x$, $\min\{\Delta N^2\}$ does not decrease significantly from its initial value for simulations with $A \lesssim 0.043$. When $A = 0.086$, $\min\{\Delta N^2\}/N_0^2$ is less than -1, meaning that overturning occurs initially. Nonetheless, $\min\{\Delta N^2\}/N_0^2$ does not vary greatly over the first 8 buoyancy periods.

The plots above demonstrate that, although overturning occurs when $\min\{\Delta N^2\} < -N_0^2$, this does not guarantee the simultaneous rapid growth of density gradients due to convective instability. The simulation results are consistent with the breaking condition of (2.32), which states that overturning is not a sufficient criterion for convective instability to occur; the background waves must evolve on a sufficiently slow timescale for overturning regions to grow in amplitude.

If the waves are close to overturning, they remain so for many buoyancy periods if $\Theta > 35^\circ$ (e.g. when $k_z = -2.5k_x$). However, if $\Theta \lesssim 35^\circ$ (e.g. when $k_z = -0.4k_x$) then the amplitude of the waves increases (and hence $\min\{\Delta N^2\}$ decreases) in part due to modulational instability.

But the rapid decrease in $\min\{\Delta N^2\}$ cannot be explained in terms of modulational instablity alone. Table 2 lists values of $\min\{\Delta N^2\}$ at times $t = T$ and $t = 4T$ determined from five simulations of different amplitude wavepackets with $k_z = -0.4k_x$. Assuming the amplitude of the waves is proportional to the value of $\min\{\Delta N^2\}$ (e.g. in linear theory, the relationship is represented explicitly by (2.28)), the growth rate, σ, of the waves is estimated by

$$\sigma \simeq \frac{1}{3T}\frac{(\min\{\Delta N^2\}|_{t=4T} - \min\{\Delta N^2\}|_{t=T})}{\min\{\Delta N^2\}|_{t=T}}. \tag{5.1}$$

The growth rate is estimated over the interval $T \leqslant t \leqslant 4T$ because during this time $\min\{\Delta N^2\}$ decreases monotonically at a steady rate in all five simulations.

If a wavepacket is unstable to weakly nonlinear modulations alone, the growth rate to lowest order is proportional to the amplitude as expressed by (2.21), However, as a function of increasing amplitude A, the growth rate listed in table 2 increases faster than linearly. Indeed, a least-square fit line to a log–log plot of the data gives the dependence

$$\sigma \propto A^{3.0\pm0.4}.$$

Spectral energy transfer diagnostics reveal that the waves grow in amplitude as a result of interactions with the wave-induced mean flow. Thus the instability occurs

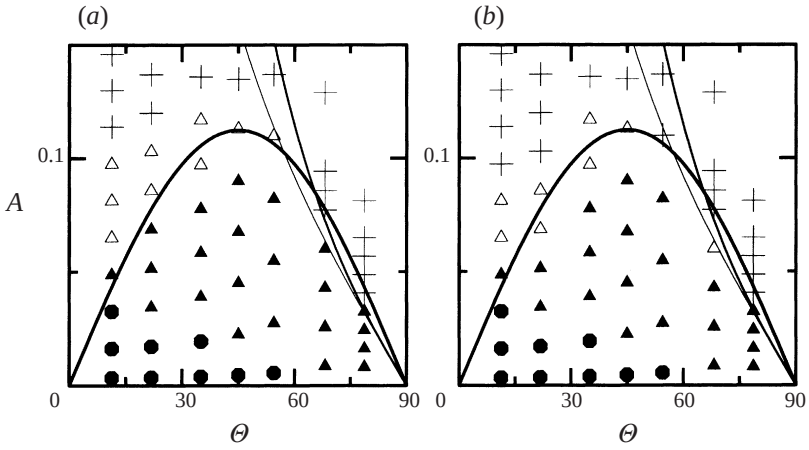

FIGURE 14. Stability regimes compared with simulation results of horizontally periodic waves with vertical extents given by (*a*) $\sigma_z k_x = 10$ and (*b*) $\sigma_z k_x = 40$. Each points represents the results of a single simulation for a wavepacket with $\Theta = \tan^{-1}(|k_z/k_x|)$ and amplitude $A = A_\xi/\lambda_x$. A solid circle denotes simulations for which $\min\{\Delta N^2\}/N_0^2 > -0.1$ over the duration of the simulation ($0 \leqslant t \lesssim 16T$). A solid triangle is plotted if $-1 < \min\{\Delta N^2\}/N_0^2 < -0.1$ over the duration of the simulation. An open triangle is plotted if $\min\{\Delta N^2\}/N_0^2 < -1$ between times $5T$ and $16T$. A cross indicates simulations in which $\min\{\Delta N^2\}/N_0^2 < -1$ before time $5T$. Superimposed on the regime diagram are the theoretically predicted stability regimes, reproduced from figure 3.

due to self-acceleration. If the amplitude of the initial wavepacket is not too large, the growth rate decreases to zero after a finite time. However, if the wavepacket is of sufficiently large amplitude initially, it may grow to such amplitude that it overturns. Whether the waves ultimately grow to such amplitude that they overturn is well represented by the self-acceleration condition (2.33). To demonstrate this, a series of simulations have been performed to examine under which conditions overturning ultimately occurs. For each simulation, the minimum value of the ΔN^2 field is determined as it evolves up to time $t \simeq 16T$.

The results for horizontally periodic waves are plotted in figure 14. In both diagrams, the symbols (circles, triangles and crosses) are plotted at the position corresponding to Θ and the normalized amplitude $A = A_\xi/\lambda_x$ of the initial wavepacket. Solid circles and triangles are plotted if the wavepacket does not overturn at any time during the simulation. Open triangles are plotted if the wavepacket is overturning after time $t = 5T$, and crosses are plotted if the wavepacket is overturning before then.

The data are plotted in figures 14(*a*) and 14(*b*) for simulations of wavepackets with vertical extent $\sigma_z = 10/k_x$ and $40/k_x$, respectively. Superimposed on the data is a heavy curve indicating the predicted boundary between stable, small-amplitude wavepackets and wavepackets that eventually overturn due to the effects of self-acceleration, as given by (2.33). The light solid curves indicate the regions where the initial wavepackets are overturning and breaking. Both diagrams show remarkably good agreement between the results of simulations and theory. The waves are stable in the linear regime and, in general, they are unstable when the self-acceleration condition is satisfied. If $\Theta \lesssim 45°$, the waves become unstable even though the amplitude of the initial wavepacket is well below that for initially overturning waves.

Similarly, a series of simulations have been performed to examine the stability characteristics of horizontally compact wavepackets. Each diagram in figure 15 is similar to those in figure 14. In figure 15(*a*), the horizontal and vertical extent of the

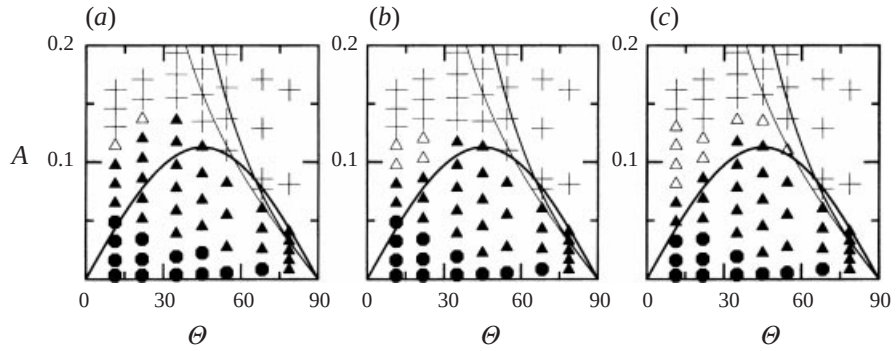

FIGURE 15. As in figure 14 but showing stability regimes for horizontally compact waves with horizontal and vertical extents given by $(\sigma_x, \sigma_z)k_x = (a)\ (10, 10)$, $(b)\ (40, 10)$ and $(c)\ (10, 40)$.

wavepacket are given by $\sigma_x = \sigma_z = 10/k_x$, in figure 15($b$) $\sigma_x = 40/k_x$ and $\sigma_z = 10/k_x$, and in figure 15(c) $\sigma_x = 10/k_x$ and $\sigma_z = 40/k_x$. The first diagram shows that waves with small Θ are stable for larger amplitudes than predicted by the self-acceleration condition, but nonetheless are unstable at amplitudes well below that of waves that are initially overturning. For wavepackets of larger horizontal or vertical extent, the stability regimes more closely correspond to that given by the self-acceleration condition.

6. Discussion and conclusions

The numerical simulations show that, in agreement with theory, quasi-plane internal wavepackets become convectively unstable even though their initial amplitude is well below that of overturning waves. The instability results from interactions between the waves and the wave-induced mean flow: the self-acceleration of the waves. This weakly nonlinear effect acts to shift the phase speed of the waves in regions where the amplitude of the waves is sufficiently large. Over time the lines of constant phase of the waves tilt more vertically in the region where the effects of self-acceleration are significant. At the boundary of this region the lines tilt more horizontally. Typically it is on the trailing edge of the wavepacket where the lines tilt more horizontally and where the waves are of sufficiently large amplitude that the waves overturn and convectively mix.

The critical amplitude for instability due to self-acceleration is given by (2.33). Numerical simulations show that the self-acceleration condition provides a good prediction of the stability boundary of horizontally periodic waves. In particular, it shows that waves with $\Theta \simeq 0$ are stable only if the amplitudes are infinitesimally small, and that waves with $\Theta \simeq 45^\circ$ are stable for the largest amplitudes. If the waves are horizontally compact, the self-acceleration condition does a poorer job of predicting the stability boundary owing to horizontal modulations of the wavepacket. Consistent with near-linear modulational stability theory, the wavepacket subdivides if $\Theta \lesssim 53^\circ$ and the wavepackets remain stable for larger initial amplitudes. Numerical simulations show that the largest amplitude horizontally compact wavepackets that are stable occur for $\Theta \simeq 35^\circ(\pm 5^\circ)$.

These results may explain why, in many laboratory experiments on internal waves generated by turbulence (for example, see Linden 1975; Sutherland & Linden 1998), the phase lines of the waves are predominantly observed to be tilted within a narrow

range of angles Θ to the vertical. At the boundary between the turbulent mixing region and the stable, unmixed region where internal waves propagate, a broad frequency spectrum occurs due to turbulent eddies deforming the boundary. One might expect a similarly broad frequency spectrum of internal waves to be generated at this boundary. However, for reasons that are not fully understood, internal waves are observed with a small range of frequencies corresponding to values of Θ lying approximately between 30° and 45°. In the light of the simulation results, it is possible that the waves of smaller and greater frequencies are not observed since these are unstable at all but negligibly small amplitudes. Experiments are currently in progress which will attempt to observe and quantify the regimes of internal wave stability under the effects of self-acceleration.

The author is indebted to the reviewers for their useful comments on the organization of the paper and, in particular, for suggesting that instability due to self-acceleration be compared with parametric instability. Many of the calculations reported here have been performed on a 40-node SGI Origin 2000 operated by the MACI community. The research has been funded in part by NSERC grant 203065-99.

Appendix A. Weakly nonlinear theory

Here the nonlinear Schrödinger equation is derived which governs the modulation of a vertically compact, horizontally periodic packet of Boussinesq internal waves. Using this equation, the stability of the wavepacket is assessed. Though less detail is given here, the derivation described below is similar to that of Grimshaw (1977), who determined the equations describing the horizontal modulations of Boussinesq and anelastic internal waves.

The fully nonlinear system of equations of two-dimensional uniformly stratified Boussinesq fluid motion is given by (2.2) and (2.3). These may be combined into a single equation of the form

$$L\psi = M, \tag{A 1}$$

where L and M are linear and nonlinear operators, respectively, acting on the streamfunction ψ. Explicitly,

$$L = L(\partial_x, \partial_z, \partial_t) = \partial_t^2 \left(\partial_x^2 + \partial_z^2\right) + N_0^2 \partial_x^2, \tag{A 2}$$

and

$$M = \nabla \cdot \left(\frac{\partial}{\partial t}(\boldsymbol{u}\zeta) + N_0^2 \frac{\partial}{\partial x}(\boldsymbol{u}\xi) \right). \tag{A 3}$$

We assume that the streamfunction is horizontally periodic though the envelope of the wavepacket may exhibit slowly varying structure vertically in space and in time. Thus to lowest order the streamfunction is

$$\psi_1^{(0)} = \alpha A(Z^\star, T^\star) \mathrm{e}^{\mathrm{i}(kx+mz-\omega t)} + \text{c.c.}, \tag{A 4}$$

where $\boldsymbol{k} = (k, m)$ is the wavenumber vector and ω is the frequency. The wavepacket envelope A is a function of the slowly varying variables $Z^\star = z/\epsilon$ and $T^\star = t/\epsilon$, where $\epsilon \ll 1$. The small, but finite amplitude $\alpha \ll 1$ of the waves is set so that $|A|$ is $O(1)$ with respect to α and ϵ. Our objective is to find a weakly nonlinear equation for A using (A 2) and (A 3). To do so, it turns out to be appropriate to set $\alpha = \epsilon$ in order to balance the lowest-order nonlinear terms.

Combining (A 4) with (A 2) gives

$$L(\partial_x, \partial_z, \partial_t)\psi_1^{(0)} = \alpha e^{i(kx+mz-\omega t)} L\left(ik, im + \epsilon\frac{\partial}{\partial Z^\star}, -i\omega + \epsilon\frac{\partial}{\partial T^\star}\right) A + \text{c.c.} \tag{A 5}$$

Expanding the operator in ϵ, we find that

$$LA = L|_{\epsilon=0}A + \epsilon L_{\mathscr{Z}}|_{\epsilon=0}\frac{\partial A}{\partial Z^\star} + \epsilon L_{\mathscr{T}}|_{\epsilon=0}\frac{\partial A}{\partial T^\star} + \tfrac{1}{2}\epsilon^2 L_{\mathscr{Z}\mathscr{Z}}|_{\epsilon=0}\frac{\partial^2 A}{\partial Z^{\star 2}} + \ldots \tag{A 6}$$

where $L_{\mathscr{Z}}$ and $L_{\mathscr{T}}$ denote partial derivatives with respect to the second and third arguments of L, respectively. Note that second derivatives involving $T^\star$ are not written explicitly because, as shown below, after a change of variables, these terms are found to be negligibly small.

Putting (A 4) and (A 6) in (A 1), and noting that the nonlinear operator M is at least of order α^2, we find we must have $L|_{\epsilon=0}A = 0$. Rigorously, this is a consequence of the compatibility condition:

$$\frac{k}{2\pi}\int_0^{2\pi/k} e^{-ikx} L|_{\epsilon=0}\alpha A(Z^\star, T^\star)e^{i(kx+mz-\omega t)}\,dx = 0. \tag{A 7}$$

Substituting $L|_{\epsilon=0} = L(ik, im, -i\omega)$ in (A 2) thereby gives the linear dispersion relation for Boussinesq internal waves: $D(k, m, \omega) = 0$, where D is defined by

$$D(k, m, \omega) \equiv L(ik, im, -i\omega) = \omega^2(k^2 + m^2) - N_0^2 k^2. \tag{A 8}$$

It is convenient to use this definition to rewrite (A 6) in terms of D:

$$LA = -i\epsilon D_m\frac{\partial A}{\partial Z^\star} + i\epsilon D_\omega\frac{\partial A}{\partial T^\star} + -\tfrac{1}{2}\epsilon^2 D_{mm}\frac{\partial^2 A}{\partial Z^{\star 2}} + \ldots. \tag{A 9}$$

Taking the first and second m-derivatives of (A 8), it is found that $D_m = c_{gz}D_\omega$, $D_{m\omega} + c_{gz}D_{\omega\omega} = 0$, and $D_{mm} = -D_\omega \partial c_{gz}/\partial m$, in which c_{gz} is the vertical group velocity of linear theory. From the dispersion relation, it is convenient to define the frequency as a function of m alone with k held fixed, i.e. $\omega_0(m; k) = N_0 k/|\boldsymbol{k}|$, in which case we have $D_{mm} = -D_\omega \omega_0''$.

These properties suggest a transformation to a coordinate system moving at the vertical group velocity. Specifically, we define $Z = Z^\star - c_{gz}T^\star = \epsilon(z - c_{gz}t)$, and $T = \epsilon T^\star = \epsilon^2 t$. In (Z, T) coordinates (A 9) becomes

$$LA = \epsilon^2 D_\omega(iA_T + \tfrac{1}{2}\omega_0'' A_{ZZ}) + O(\epsilon^2\alpha, \epsilon^3). \tag{A 10}$$

Thus the left-hand side of (A 1) is $O(\alpha\epsilon^2)$. If the amplitude of the waves is infinitesimally small, if $\alpha \ll \epsilon$, the right-hand side of this equation is negligible. The resulting equation, to lowest order, is the linear Schrödinger equation:

$$iA_T + \tfrac{1}{2}\omega_0'' A_{ZZ} = 0, \tag{A 11}$$

which describes modulations of the wavepackets under the effects of linear dispersion.

If the amplitude is not negligible but $\alpha \sim \epsilon$, then the weakly nonlinear effects, given by (A 3), are balanced by second-order dispersion effects, given by (A 6), both of which are of order $\alpha^3 \sim \alpha\epsilon^2$. Explicitly, to lowest order the compatibility condition determined from (A 1) is

$$\alpha\epsilon^2 e^{i(mz-\omega t)}(iA_T + \tfrac{1}{2}\omega_0'' A_{ZZ}) = \frac{1}{D_\omega}\frac{k}{2\pi}\int_0^{2\pi/k} e^{-ikx} M_1\,dx, \tag{A 12}$$

where M_1 is determined from (A 3) at order α^3. In theory, weakly nonlinear effects occur due to two types of interactions: those between waves of wavenumber k and the wave-induced mean flow, and those between waves of wavenumber k and $2k$. For quasi-plane wavepackets, only the former is significant to lowest order, as demonstrated by figures 10 and 11.

The wave-induced mean flow is given to order α^2 by the pseudomomentum, (2.17). Denoting the wave-induced mean flow by u_0 and using (A 4), we find

$$u_0 = -\langle \zeta \xi \rangle = 2(k^2 + m^2)(k/\omega)\alpha^2 |A|^2 + O(\epsilon\alpha^2, \alpha^4). \tag{A 13}$$

From this equation and the conservation of mass, it is found that the mean horizontal values of ζ, ξ and w are zero at this order. Therefore

$$M_1 = \frac{\partial}{\partial x}\left(\frac{\partial}{\partial t}(u_0 \zeta_1^{(0)}) + N_0^2 \frac{\partial}{\partial x}(u_0 \xi_1^{(0)})\right), \tag{A 14}$$

where ${\zeta_1}^{(0)}$ and $\xi_1^{(0)}$ are the vorticity and vertical displacement fields, respectively, which are determined from the first term on the right-hand side of (A 4).

Substituting this expression in (A 12), after some algebra the right-hand side of the equation is found to be

$$\alpha^3 \frac{1}{D_\omega}(4|\boldsymbol{k}|^4 k^2)|A|^2 A \mathrm{e}^{\mathrm{i}(mz - \omega t)} \tag{A 15}$$

and so (A 12) can be written in the standard form of the one-dimensional nonlinear Schrödinger equation

$$\mathrm{i}A_T + \tfrac{1}{2}\omega_0'' A_{ZZ} + \gamma |A|^2 A = 0, \tag{A 16}$$

where

$$\gamma = -2\omega_0 |\boldsymbol{k}|^4 / N_0^2. \tag{A 17}$$

It follows from (A 16) that the nonlinear dispersion relation for vertical modulations of horizontally periodic internal waves is given by

$$\omega = \omega_0(1 + 2|\boldsymbol{k}|^4 / N_0^2 \alpha^2) + O(\alpha^4). \tag{A 18}$$

Identifying α with the streamfunction amplitude A_0 (e.g. as in (2.11)), the dispersion relation given to second order in the amplitude $A = A_\xi / \lambda_x$ is

$$\omega = \omega_0(1 + 2\pi^2 A^2 / \cos^2 \Theta). \tag{A 19}$$

Appendix B. Deep water theory

It is instructive to compare the stability conditions for internal waves with those for surface waves on deep water. In this case, the wave-induced mean flow M_{SW} is given by the 'Stokes drift', A_M. Explicitly, to second order in the amplitude,

$$A_M = \omega k_x A^2 \lambda^2, \tag{B 1}$$

in which ω is the frequency, k_x is the horizontal wavenumber, and A is the ratio of the maximum vertical displacement of the waves to the horizontal wavelength.

The analogous self-acceleration condition for surface waves states that interactions between the waves and the wave-induced mean flow is significant if the Stokes drift is larger than the horizontal group velocity c_{gx}. Using the dispersion relationship for deep water waves, the self-acceleration condition is

$$A = A_\xi / \lambda_x > \frac{1}{2\pi\sqrt{2}} \simeq 0.11. \tag{B 2}$$

As in the case of internal waves, the amplitude necessary for the effect of self-acceleration to be significant is an order of magnitude smaller than horizontal wavelength.

However, for deep water waves, the maximum amplitude the waves can attain before forming a cusp and breaking is $A_{\max} \simeq 0.0706$ (Lighthill 1978). Thus, to the order of approximation used here to formulate the self-acceleration condition, deep water waves cannot become unstable under the effects of self-acceleration. Nor does it seem that large-amplitude effects should change this conclusion. The nonlinear dispersion relation for deep water waves is $\omega = (gk)^{1/2}[1 + A_\xi^2 k^2/2 + O(A^4)]$ (e.g. see Whitham 1974, § 13.13). Thus the second-order term is at most $2(\pi A_{\max})^2 \simeq 0.1$, an order of magnitude smaller than the leading term in the dispersion relation.

That is not to say that deep water waves are stable below breaking amplitudes: using the variational approach by Whitham (1965), Lighthill (1967) showed that finite-amplitude deep water waves are always unstable due to weakly nonlinear modulations of the wavepacket, though such instability does not necessarily result in wave breaking.

Appendix C. Spectral energy transfers

The transfer of energy between different Fourier modes has been used to analyse two-dimensional isotropic turbulence (e.g. Herring *et al.* 1974), and the growth and nonlinear development of parallel flow instabilities in density-stratified fluid (Smyth & Peltier 1992; Sutherland & Peltier 1994).

In the discussion below, diffusive effects are assumed to be negligible. Energy is thus redistributed due to nonlinear advection, but the total energy in the domain remains approximately constant.

The change in energy due to advection is given by

$$\frac{\partial \mathscr{E}}{\partial t} = -\nabla \cdot (\boldsymbol{u}\mathscr{E}) \tag{C 1}$$

where the energy per unit mass is

$$\mathscr{E} = -\tfrac{1}{2}(|\boldsymbol{u}|^2 + N_0^2 \xi^2) \tag{C 2}$$

(e.g. Gill 1982). The basic-state fields at a particular time are Fourier decomposed so that, for example, $\xi(x,z) = \sum_{\boldsymbol{k}} \hat{\xi}_{\boldsymbol{k}} \exp(-\mathrm{i}\boldsymbol{k}\cdot\boldsymbol{x})$, where $\hat{\xi}$ is the amplitude of the Fourier mode with wavenumber $\boldsymbol{k} = (k, m)$.

Using (2.5) and (2.6), the velocity fields are written in terms of the Fourier decomposition of the streamfunction $\psi(x,z) = \sum_{\boldsymbol{k}} \hat{\psi}_{\boldsymbol{k}} \exp(-\mathrm{i}\boldsymbol{k}\cdot\boldsymbol{x})$. To ensure the fields are real-valued $\hat{\psi}_{(-k,m)} = \hat{\psi}^\star_{(k,m)}$, where the star denotes the complex conjugate.

Substituting these equations into (C 1) and (C 2) gives

$$\frac{\partial \mathscr{E}_{\boldsymbol{k}}}{\partial t} = \mathscr{F}_{\boldsymbol{k}} \tag{C 3}$$

where

$$\mathscr{F}_{\boldsymbol{k}} = -\tfrac{1}{2}\psi^\star_{\boldsymbol{k}} \sum_{\boldsymbol{k}'} \mathscr{T}^{\mathrm{KE}}(\boldsymbol{k},\boldsymbol{k}') - \tfrac{1}{2} N_0^2 \xi^\star_{\boldsymbol{k}} \sum_{\boldsymbol{k}'} \mathscr{T}^{\mathrm{APE}}(\boldsymbol{k},\boldsymbol{k}'), \tag{C 4}$$

$$\mathscr{T}^{\mathrm{KE}}(\boldsymbol{k},\boldsymbol{k}') = |\boldsymbol{k}'|^2 (mk' - km')\psi_{\boldsymbol{k}-\boldsymbol{k}'}\psi_{\boldsymbol{k}'} + \text{c.c.}, \tag{C 5}$$

$$\mathscr{T}^{\mathrm{APE}}(\boldsymbol{k},\boldsymbol{k}') = (mk' - km')\psi_{\boldsymbol{k}-\boldsymbol{k}'}\xi_{\boldsymbol{k}'} + \text{c.c.}, \tag{C 6}$$

in which $\boldsymbol{k}' = (k', m')$. Thus the energy in the Fourier mode $\boldsymbol{k}$ changes as a result of the sum of interactions between the mode pairs $\boldsymbol{k}'$ and $\boldsymbol{k} - \boldsymbol{k}'$.

At regular intervals during a simulation the discrete Fourier transform coefficients $\psi_{\boldsymbol{k}}$ and $\xi\boldsymbol{k}$ are determined using a standard FFT algorithm (Press *et al.* 1993). The sums in (C 4) are then computed. The numerical accuracy of this procedure is tested by evaluating the sum $\sum_{\boldsymbol{k}} \mathscr{F}_{\boldsymbol{k}}$. As expected it is found to be negligibly small during numerical simulations of propagating waves.

The normalized transfer of energy between waves and the mean flow is diagnosed by partitioning the sums in (C 4) into two parts:

$$\mathscr{F}^0_{\boldsymbol{k}} = -\tfrac{1}{2}\psi^\star_{\boldsymbol{k}} \sum_{m'} \mathscr{T}^{\mathrm{KE}}(\boldsymbol{k}, (0, m')) - \tfrac{1}{2} N_0^2 \xi^\star_{\boldsymbol{k}} \sum_{m'} \mathscr{T}^{\mathrm{APE}}(\boldsymbol{k}, (0, m')), \tag{C 7}$$

and

$$\mathscr{F}'_{\boldsymbol{k}} = -\tfrac{1}{2}\psi^\star_{\boldsymbol{k}} \sum_{\boldsymbol{k}', k' \neq 0} \mathscr{T}^{\mathrm{KE}}(\boldsymbol{k}, \boldsymbol{k}') - \tfrac{1}{2} N_0^2 \xi^\star_{\boldsymbol{k}} \sum_{\boldsymbol{k}', k' \neq 0} \mathscr{T}^{\mathrm{APE}}(\boldsymbol{k}, \boldsymbol{k}'). \tag{C 8}$$

The former equation corresponds to spectral energy transfers into mode $\boldsymbol{k}$ due to wave-mean flow interactions. The latter equation corresponds to spectral energy transfers into mode $\boldsymbol{k}$ due to wave–wave interactions.

The normalized spectral transfer of energy from waves to the mean flow is thus defined to be

$$T_{W0} = \sum_m \mathscr{F}'_{(0,m)} / 2\mathscr{E}, \tag{C 9}$$

where $\mathscr{E}$ is given by (C 2). Similarly the transfer of energy from waves to the mode with horizontal wavenumber nk_x is defined by

$$T_{Wn} = \sum_m \mathscr{F}'_{(nk_x,m)} / 2\mathscr{E}. \tag{C 10}$$

The extraction of energy from the mean flow into the mode with horizontal wavenumber nk_x is defined by

$$T_{0n} = \sum_m \mathscr{F}^0_{(nk_x,m)} / 2\mathscr{E}. \tag{C 11}$$

These three forms of the normalized spectral energy transfer rates are used to produce figures 10 and 11.

REFERENCES

Arnol'd, V. I. 1969 On an *a priori* estimate in the theory of hydrodynamical stability. *Am. Math. Soc. Transl.* (2) **79**, 267–269.

Benielli, D. & Sommeria, J. 1996 Excitation of internal waves and stratified turbulence by parametric instability. *Dyn. Atmos. Oceans* **23**, 335–343.

Benjamin, T. B. 1967 Internal waves of permanent form in fluids of great depth. *J. Fluid Mech.* **29**, 559–592.

Benjamin, T. B. & Feir, J. E. 1967 The disintegration of wavetrains on deep water. *J. Fluid Mech.* **27**, 417–430.

Booker, J. R. & Bretherton, F. P. 1967 The critical layer for internal gravity waves in shear flow. *J. Fluid Mech.* **27**, 513–539.

Bouruet-Aubertot, P., Sommeria, J. & Staquet, C. 1995 Instabilities and breaking of standing internal gravity waves. *J. Fluid Mech.* **285**, 265–301.

Breeding, R. J. 1972 A nonlinear model of the break-up of internal gravity waves due to their exponential growth with height. *J. Geophys. Res.* **77**, 2681–2692.

Bretherton, F. P. 1966 Gravity waves in shear. *Q. J. R. Met. Soc.* **92**, 466–480.

Broad, A. S. 1995 Linear theory of momentum fluxes in 3-D flows with turning of the mean wind with height. *Q. J. R. Met. Soc.* **121**, 1891–1902.

Broad, A. S. 1999 Do orographic gravity waves break in flows with uniform wind direction turning with height? *Q. J. R. Met. Soc.* **125**, 1695–1714.

Debnath, L. 1994 *Nonlinear Water Waves.* Academic.

Drazin, P. G. 1977 On the instability of an internal gravity wave. *Proc. R. Soc. Lond.* A **356**, 411–432.

Drazin, P. G. & Reid, W. H. 1981 *Hydrodynamic Stability*. Cambridge University Press.

Dunkerton, T. J. 1981 Wave transience in a compressible atmosphere. Part I: Transient internal wave, mean-flow interaction. *J. Atmos. Sci.* **38**, 281–297.

Dunkerton, T. J. 1982 Wave transience in a compressible atmosphere. Part III: The saturation of internal gravity waves in the mesosphere. *J. Atmos. Sci.* **39**, 1042–1051.

Dunkerton, T. J. 1989 Theory of internal gravity wave saturation. *Pure Appl. Geophys.* **130**, 373–397.

Eliassen, A. & Palm, E. 1961 On the transfer of energy in stationary mountain waves. *Geofys. Publ.* **22**, 1–23.

Fermi, E., Pasta, J. & Ulam, S. 1974 Studies of nonlinear problems I, Los Alamos Report LA 1940, 1955. In *Reproduced in Nonlinear Wave Motion* (ed. A. C. Newell). Providence, RI: Am. Math. Soc.

Fritts, D. C. 1978 The nonlinear gravity wave-critical level interation. *J. Atmos. Sci.* **35**, 397–413.

Fritts, D. C. 1982 Shear excitation of atmospheric gravity waves. *J. Atmos. Sci.* **39**, 1936–1952.

Fritts, D. C. & Dunkerton, T. J. 1984 A quasi-linear study of gravity-wave saturation and self-acceleration. *J. Atmos. Sci.* **41**, 3272–3289.

Fritts, D. C. & Rastogi, P. K. 1985 Convective and dynamical instabilities due to gravity wave motions in the lower and middle atmosphere: Theory and observations. *Radio Sci.* **20**, 1247–1277.

Gill, A. E. 1982 *Atmosphere-Ocean Dynamics.* Academic.

Grimshaw, R. H. J. 1975*a* Nonlinear internal gravity waves and their interaction with the mean wind. *J. Atmos. Sci.* **32**, 1779–1793.

Grimshaw, R. H. J. 1975*b* The modulation and stability of an internal gravity wave. *Tech. Rep.* 32, Department of Mathematical Sciences, University of Melbourne.

Grimshaw, R. H. J. 1977 The modulation of an internal gravity-wave packet, and the resonance with the mean motion. *Stud. Appl. Maths* **56**, 241–266.

Hasselmann, K. 1967 A criterion for non-linear wave stability. *J. Fluid Mech.* **30**, 737–739.

Herring, J. R., Orszag, S. A., Kraichnan, R. H. & Fox, D. G. 1974 Decay of two-dimensional homogeneous turbulence. *J. Fluid. Mech.* **66**, 417–444.

Jones, W. L. & Houghton, D. D. 1971 The coupling of momentum between internal gravity waves and mean flow: A numerical study. *J. Atmos. Sci.* **28**, 604–608.

Jones, W. L. & Houghton, D. D. 1972 The self-destructing internal gravity wave. *J. Atmos. Sci.* **29**, 844–849.

Klostermeyer, J. 1991 Two- and three-dimensional parametric instabilities in finite amplitude internal gravity waves. *Geophys. Astrophys. Fluid Dyn.* **64**, 1–25.

Lake, B. M., Yuen, H. C., Rundgaldier, H. & Ferguson, W. E. 1977 Nonlinear deep-water waves: Theory and experiment. Part 2. Evolution of a continuous wave train. *J. Fluid Mech.* **83**, 49–74.

Lighthill, M. J. 1967 Some special cases treated by the Whitham theory. *Proc. R. Soc. Lond.* A **299**, 38–53.

Lighthill, M. J. 1978 *Waves in Fluids.* Cambridge University Press.

Linden, P. F. 1975 The deepening of a mixed layer in a stratified fluid. *J. Fluid Mech.* **71**, 385–405.

Lombard, P. N. & Riley, J. J. 1996 On the breakdown into turbulence of propagating internal waves. *Dyn. Atmos. Ocean* **23**, 345–355.

McIntyre, M. E. 1973 Mean motions and impulse of a guided internal gravity wave packet. *J. Fluid Mech.* **60**, 801–811.

McIntyre, M. E. & Weissman, M. A. 1978 On radiating instabilities and resonant overreflection. *J. Atmos. Sci.* **35**, 1190–1196.

Mied, R. R. 1976 The occurrence of parametric instabilities in finite-amplitude internal gravity waves. *J. Fluid Mech.* **78**, 763–784.

Phillips, O. M. 1981 Wave interactions – the evolution of an idea. *J. Fluid Mech.* **106**, 215–227.

Press, W. H., Flannery, B. P., Teukolsky, S. A. & Vetterling, W. T. 1993 *Numerical Recipes: The Art of Scientific Computing*, 2nd Edn. Cambridge University Press.

Rayleigh, Lord 1883 Investigation of the character of the equilibrium of an incompressible heavy fluid of variable density. *Proc. Lond. Math. Soc.* **14**, 170–177.

Ripa, P. 1991 General stability conditions for a multi-layer model. *J. Fluid Mech.* **222**, 119–137.

Scinocca, J. F. & Shepherd, T. G. 1992 Nonlinear wave-activity conservation laws and Hamiltonian structure for the two-dimensional anelastic equations. *J. Atmos. Sci.* **49**, 5–27.

Shepherd, T. G. 1990 Symmetries, conservation laws, and Hamiltonian structure in geophysical fluid dynamics. *Adv. Geophys.* **32**, 287–338.

Shutts, G. J. 1995 Gravity-wave drag parametrization over complex terrain: the effect of critical level absorption in directional wind shear. *Q. J. R. Met. Soc.* **121**, 1005–1021.

Shutts, G. J. 1998 Stationary gravity-wave structure in flows with directional wind shear. *Q. J. R. Met. Soc.* **124**, 1421–1442.

Smyth, W. D. & Peltier, W. R. 1992 Spectral transfers in 2d anisotropic flow. *Phys. Fluids* A **4**, 340–349.

Smyth, W. D. & Peltier, W. R. 1993 Two dimensional turbulence in homogeneous and stratified shear layers. *Geophys. Astrophys. Fluid Dyn.* **69**, 1–32.

Spiegel, E. A. & Veronis, G. 1960 On the Boussinesq approximation for a compressible fluid. *Astrophys. J.* **131**, 442–447.

Sutherland, B. R. 1996 Internal gravity wave radiation into weakly stratified fluid. *Phys. Fluids* **8**, 430–441.

Sutherland, B. R. 1999 Propagation and reflection of large amplitude internal gravity waves. *Phys. Fluids* **11**, 1081–1090.

Sutherland, B. R. 2000 Internal wave reflection in uniform shear. *Q. J. R. Met. Soc.* **126**, 3255–3287.

Sutherland, B. R., Caulfield, C. P. & Peltier, W. R. 1994 Internal wave generation and hydrodynamic instability. *J. Atmos. Sci.* **51**, 3261–3280.

Sutherland, B. R. & Linden, P. F. 1998 Internal wave generation by flow over a thin barrier. *J. Fluid Mech.* **377**, 223–252.

Sutherland, B. R. & Peltier, W. R. 1994 Turbulence transition and internal wave generation in density stratified jets. *Phys. Fluids* A **6**, 1267–1284.

Taylor, G. I. 1950 The instability of liquid surfaces when accelerated in a direction perpendicular to their planes. *Proc. R. Soc. Lond.* A **201**, 192–196.

Walterscheid, R. L. 1984 Gravity wave attenuation and the evolution of the mean state following wave breakdown. In *Dynamics of the Middle Atmosphere* (ed. J. R. Holton & T. Matsuno), pp. 19–43. Terra Scientific Publishing,

Whitham, G. B. 1965 A general approach to linear and nonlinear dispersive waves using a Lagrangian. *J. Fluid. Mech.* **22**, 273–283.

Whitham, G. B. 1967 Nonlinear dispersion of water waves. *J. Fluid. Mech.* **27**, 399–412.

Whitham, G. B. 1974 *Linear and Nonlinear Waves*. John Wiley and Sons.

Zabusky, N. J. & Kruskal, M. D. 1965 Interaction of solitons in a collisionless plasma and the recurrence of initial states. *Phys. Rev. Lett.* **15**, 240–243.